LETTER

https://doi.org/10.1038/s41586-019-1030-9

Recruitment of BRCA1 limits MYCN-driven accumulation of stalled RNA polymerase

Steffi Herold[1,7]*, Jacqueline Kalb[1,7], Gabriele Büchel[1,7], Carsten P. Ade[1], Apoorva Baluapuri[2], Jiajia Xu[1], Jan Koster[3], Daniel Solvie[1], Anne Carstensen[1], Christina Klotz[1], Sabrina Rodewald[4], Christina Schülein-Völk[1], Matthias Dobbelstein[4], Elmar Wolf[2], Jan Molenaar[5], Rogier Versteeg[3], Susanne Walz[6] & Martin Eilers[1]*

MYC is an oncogenic transcription factor that binds globally to active promoters and promotes transcriptional elongation by RNA polymerase II (RNAPII)[1,2]. Deregulated expression of the paralogous protein MYCN drives the development of neuronal and neuroendocrine tumours and is often associated with a particularly poor prognosis[3]. Here we show that, similar to MYC, activation of MYCN in human neuroblastoma cells induces escape of RNAPII from promoters. If the release of RNAPII from transcriptional pause sites (pause release) fails, MYCN recruits BRCA1 to promoter-proximal regions. Recruitment of BRCA1 prevents MYCN-dependent accumulation of stalled RNAPII and enhances transcriptional activation by MYCN. Mechanistically, BRCA1 stabilizes mRNA decapping complexes and enables MYCN to suppress R-loop formation in promoter-proximal regions. Recruitment of BRCA1 requires the ubiquitin-specific protease USP11, which binds specifically to MYCN when MYCN is dephosphorylated at Thr58. USP11, BRCA1 and MYCN stabilize each other on chromatin, preventing proteasomal turnover of MYCN. Because BRCA1 is highly expressed in neuronal progenitor cells during early development[4] and MYC is less efficient than MYCN in recruiting BRCA1, our findings indicate that a cell-lineage-specific stress response enables MYCN-driven tumours to cope with deregulated RNAPII function.

To study the transcriptional function of MYCN, we expressed a MYCN–ER chimeric protein in SH-EP neuroblastoma cells, which do not express endogenous MYCN (Fig. 1a). RNA sequencing of cells treated with 4-hydroxytamoxifen (4-OHT) revealed that activation of MYCN generated an expression profile that discriminated *MYCN*-amplified neuroblastoma from non-*MYCN*-amplified tumours, independent of tumour stage (Extended Data Fig. 1a, b). The strong increase in expression of canonical MYC-activated genes in *MYCN*-amplified relative to non-amplified tumours of the same stage accounted for the difference (Extended Data Fig. 1c). *MYCN*-amplified tumours also showed suppression of genes that are specifically expressed in T cells, which probably reflects a low number of T cells in these tumours[5] (Extended Data Fig. 1c).

Activation of MYCN led to both the activation and repression of genes (Fig. 1b). Chromatin immunoprecipitation coupled with sequencing (ChIP–seq) showed that promoters of both activated and repressed genes were bound by MYCN (Extended Data Fig. 1d). MYCN-activated genes bound to more MYCN and showed higher basal expression levels than MYCN-repressed genes[6–8] (Extended Data Fig. 1d, e). Sequencing of 4-thiouridine-labelled nascent RNA showed that changes in RNA synthesis paralleled mRNA levels at steady state[6] (Fig. 1b and Extended Data Fig. 1f). Activation of MYCN caused a shift in overall RNAPII occupancy at actively expressed genes from the promoter into the gene body that has previously been observed in response to MYC[3] (Fig. 1c and Extended Data Fig. 2a, b). RNAPII occupancy data were identical whether data were read-normalized or normalized using a spike-in control (Extended Data Fig. 2c). ChIP–seq of RNAPII phosphorylated at Ser2 (RNAPII(pSer2)) confirmed that activation of MYCN caused an increase in transcriptional elongation when averaged over all genes (Extended Data Fig. 2a). Stratifying the alteration in RNAPII occupancy to MYCN activation by the change in mRNA expression showed that the decrease in RNAPII occupancy at the promoter occurred uniformly on activated, repressed and non-regulated genes, which are expressed at a similar level (Fig. 1c and Extended Data Fig. 2d). By contrast, the MYCN-dependent change in RNAPII and RNAPII(pSer2) occupancy in the body of the gene or at the transcription end site was highly regulated: RNAPII(pSer2) increased strongly on MYCN-activated genes, did not change on non-regulated genes and decreased on MYCN-repressed genes (Fig. 1d, e and Extended Data Fig. 2d). Over all genes, the amount of elongating RNAPII paralleled the MYCN-dependent change in mRNA levels (Fig. 1e). A strong G/C-skew[9] in promoter-proximal regions correlated closely with positive regulation by MYCN (Fig. 1f).

We reasoned that activation of MYCN–ER would increase the dependence on genes that control the transcriptional functions of MYCN and screened for short hairpin RNAs (shRNAs) that decrease the fitness of MYCN–ER cells in the presence—but less in the absence—of 4-OHT (Extended Data Fig. 3a). Out of a total of 12,931 shRNAs, this screen identified 104 shRNAs targeting 99 genes that were more-strongly depleted upon growth in the presence of 4-OHT (Supplementary Table 1). Notably, activation of MYCN strongly enhanced the selection against three out of the six shRNAs targeting *BRCA1* that were present in the screen (Extended Data Fig. 3b). Independent shRNAs targeting *BRCA1* suppressed colony formation more strongly in the presence of 4-OHT (Extended Data Fig. 3c, d). The expression of genes targeted by hits from this screen was enhanced in *MYCN*-amplified neuroblastomas (Extended Data Fig. 3e). Indeed, BRCA1 expression closely correlated with *MYCN* amplification (Extended Data Fig. 3f) and was a strong indicator of poor prognosis (Extended Data Fig. 3g). Available datasets of copy-number variation did not show increases in *BRCA1* in *MYCN*-amplified tumours (data not shown). By contrast, genome-wide DNA-methylation data identified *BRCA1* as the most significant differentially methylated gene in high-risk and *MYCN*-amplified neuroblastoma (Fig. 2a). Specifically, the *BRCA1* promoter was significantly hypomethylated in patients with high-risk neuroblastoma, whereas hypermethylation was observed in patients with low-risk neuroblastoma (Extended Data Fig. 3h), indicating that there is selective pressure for high BRCA1 expression in *MYCN*-amplified neuroblastoma.

Because BRCA1 stabilizes replication forks and promotes homologous recombination[10], we tested whether depletion of *BRCA1* interferes

[1]Theodor Boveri Institute, Department of Biochemistry and Molecular Biology, Biocenter, University of Würzburg, Würzburg, Germany. [2]Cancer Systems Biology Group, Department of Biochemistry and Molecular Biology, Biocenter, University of Würzburg, Würzburg, Germany. [3]Department of Oncogenomics, Academic Medical Center (AMC), University of Amsterdam, Amsterdam, The Netherlands. [4]Institute of Molecular Oncology, Göttingen Center of Molecular Biosciences, University of Göttingen, Göttingen, Germany. [5]Department of Translational Research, Prinses Máxima Centrum voor Kinderoncologie, Utrecht, The Netherlands. [6]Comprehensive Cancer Center Mainfranken, Core Unit Bioinformatics, Biocenter, University of Würzburg, Würzburg, Germany. [7]These authors contributed equally: Steffi Herold, Jacqueline Kalb, Gabriele Büchel. *e-mail: s.herold@uni-wuerzburg.de; martin.eilers@biozentrum.uni-wuerzburg.de

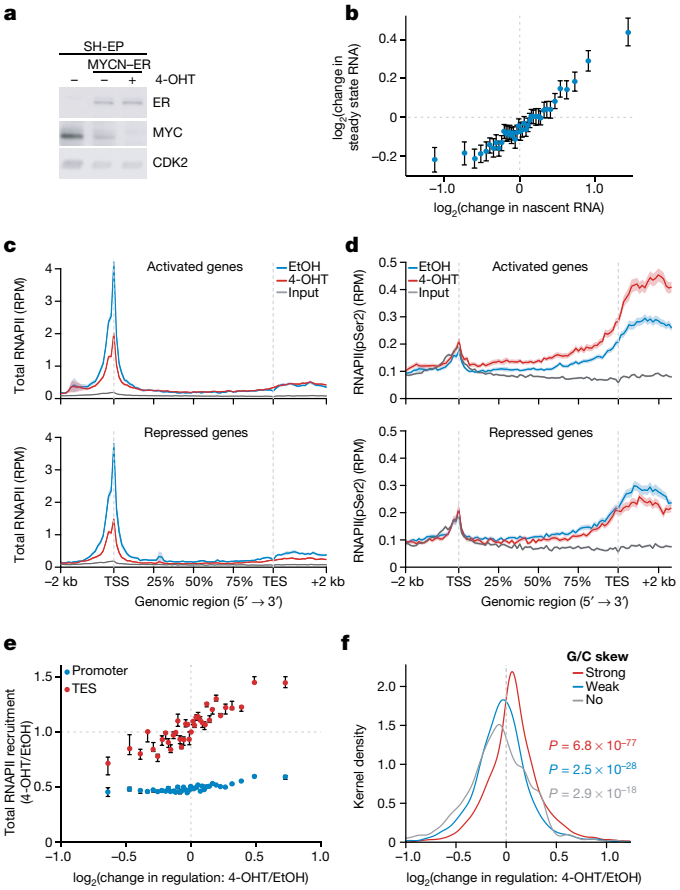

Fig. 1 | Effects of MYCN on gene expression and RNAPII function. **a**, Immunoblot documenting MYC and MYCN–ER levels in SH-EP cells. Cells were treated with 200 nM 4-OHT or ethanol for 3 h. CDK2 is used as loading control. $n = 3$; in all legends, n indicates the number of independent biological replicates. **b**, Correlation between regulation by MYCN measured by nascent and steady-state RNA levels. In total, 18,213 genes were binned. Data are mean ± 95% confidence interval. $n = 3$. **c**, Metagene plots of total RNAPII after 4-OHT treatment (3 h) for the 914 most strongly MYCN-activated (top) and 615 MYCN-repressed genes (bottom). Data are mean ± s.e.m. (indicated by the line and shading throughout). $n = 4$. EtOH, ethanol; RPM, reads per million mapped reads. TES, transcription end site; TSS, transcription start site. **d**, Metagene plots of RNAPII(pSer2) for MYCN-activated and MYCN-repressed genes. Data are mean ± s.e.m. $n = 4$. **e**, Correlation between transcriptional changes and RNAPII occupancy at promoters and transcription end sites after MYCN–ER activation. In total, 11,093 expressed genes were binned based on $\log_2$(fold change in expression). Plots show median ± bootstrapped 95% confidence intervals of 1,000 resamplings. **f**, Kernel density plot of regulation by MYCN of gene with promoters that have different G/C skews (strong: 4,003; weak: 3,381; no: 1,377). $n = 3$. P values were calculated with a two-tailed Wilcoxon one-sample signed-rank test with $\mu = 0$.

with DNA replication or causes double-strand breaks in a MYCN-dependent manner. Depletion of *BRCA1* slowed cell-cycle progression and led to an increase in cells in the G1 phase of the cell cycle (Extended Data Fig. 4a, b). Staining with 5-bromo-2′-deoxyuridine (BrdU) showed that *BRCA1* depletion reduced the percentage of cells in S phase and that activation of MYCN–ER stimulated S-phase entry in both control and *BRCA1*-depleted cells (Extended Data Fig. 4b). Depletion of *BRCA1* did not induce apoptosis before or after MYCN–ER activation (Extended Data Fig. 4c). DNA fibre assays showed that depletion of *BRCA1* reduced the average speed of replication fork progression, but activation of MYCN–ER had no significant effect (Extended Data Fig. 4d, e). Depletion of *BRCA1* also led to an increase in the number of γH2A.X and 53BP1 foci, which are indicators of double-stranded DNA breaks (Extended Data Fig. 4f), whereas prolonged activation of MYCN (24 h) led to only a small and statistically insignificant increase in the number of foci. This indicated that MYCN-induced perturbation of DNA replication or double-stranded breaks is unlikely to be the main reason for the increased dependence on BRCA1.

No association of BRCA1 was found with promoter-proximal regions in control cells (Fig. 2b). Activation of MYCN–ER led to a strong increase in the association of BRCA1 with promoter-proximal regions, and the extent of recruitment was equivalent to the expression of the downstream gene (Fig. 2b, c). In addition, MYCN recruited BRCA1 to intergenic sites (Extended Data Fig. 5a). BRCA1-binding sites closely overlapped with MYCN-binding sites (Fig. 2b, d). Consistently, a consensus MYC-binding sequence (E-box) was enriched around BRCA1-binding sites (Extended Data Fig. 5b) and a de novo search for DNA-binding motifs in BRCA1-binding sites identified this sequence as the most strongly enriched DNA motif upon activation of MYCN (Extended Data Fig. 5c). Both short interfering RNA (siRNA)-mediated and shRNA-mediated depletion of *BRCA1* reduced the signal observed in ChIP experiments (Extended Data Fig. 5d, e). In addition, ChIP experiments using a second anti-BRCA1 antibody confirmed the validity of the results (Extended Data Fig. 5f). Stable constitutive expression of MYCN also recruited BRCA1 to promoter-proximal regions (Extended Data Fig. 5g, h). By contrast, addition of 4-OHT to SH-EP cells that did not express MYCN–ER had no effect on chromatin occupancy of BRCA1 (Extended Data Fig. 5i).

MYCN activation strongly increased the association between BRCA1 and RNAPII phosphorylated at Ser5, whereas the association between BRCA1 and unphosphorylated RNAPII or RNAPII(pSer2) was only slightly increased[11] (Fig. 2e). Inhibition of the CDK9 kinase that phosphorylates RNAPII at Ser2 further enhanced recruitment of BRCA1 to promoters by MYCN (Fig. 2f and Extended Data Fig. 6a), and decreased recruitment to joint MYCN–BRCA1 sites that were not localized in promoters, which indicates a competition for limited pools of BRCA1[11] (Extended Data Fig. 6b). Inhibition of the CDK7 kinase that phosphorylates RNAPII at Ser5 led to only a small increase in recruitment (Extended Data Fig. 6c). Inhibition of CDK9 in IMR-5 neuroblastoma cells, which contain amplification of *MYCN*, enhanced recruitment of BRCA1 in a MYCN-dependent manner (Extended Data Fig. 6d). We conclude that stalling of RNA polymerase at the pause site strongly enhances recruitment of BRCA1 by MYCN[12].

Depletion of *BRCA1* altered the response of RNAPII to MYCN activation (Fig. 3a and Extended Data Fig. 7a). In *BRCA1*-depleted cells, MYCN activation led to an accumulation of RNAPII at the pause site instead of promoting pause release (Fig. 3a and Extended Data Fig. 7a). This was not due to BRCA1-dependent changes in phosphorylation of RNAPII (Extended Data Fig. 7b). Consistently, activation of MYCN reduced NELF-E promoter occupancy in control cells, but increased it in *BRCA1*-depleted cells (Extended Data Fig. 7c). As a consequence, activation of MYCN increased rather than decreased the travelling ratio of RNAPII in *BRCA1*-depleted cells (Extended Data Fig. 7d). A bin plot confirmed that MYCN activation broadly decreased RNAPII association within promoter-proximal regions in control cells but increased the association in *BRCA1*-depleted cells (Fig. 3b). RNAPII(pSer2) showed an increase at the termination site upon stimulation of MYCN–ER in control cells, but a decrease in *BRCA1*-depleted cells (Extended Data Fig. 7e). Consistent with these observations, depletion of *BRCA1* attenuated activation of multiple MYCN target gene sets and overall changes in gene expression in response to activation of MYCN (Extended Data Fig. 7f,g).

Because the G/C skew of promoters correlates closely with their ability to form R-loops[9] and because BRCA1 can suppress R-loop formation at promoter-proximal regions[13] and at transcription end sites[14], the data suggested that BRCA1 might suppress R-loop formation upon MYCN activation. Available datasets[15] showed that 85% of genes annotated to have promoter-proximal R-loops have joint MYCN–BRCA1 sites in promoter-proximal regions, whereas only 50% of genes with distal R-loops do (proximal: 1,328 out of 1,749 promoters; >2 kb: 1,987 out of 3,978 genes; $P < 0.0001$). Notably, promoters in which MYCN is

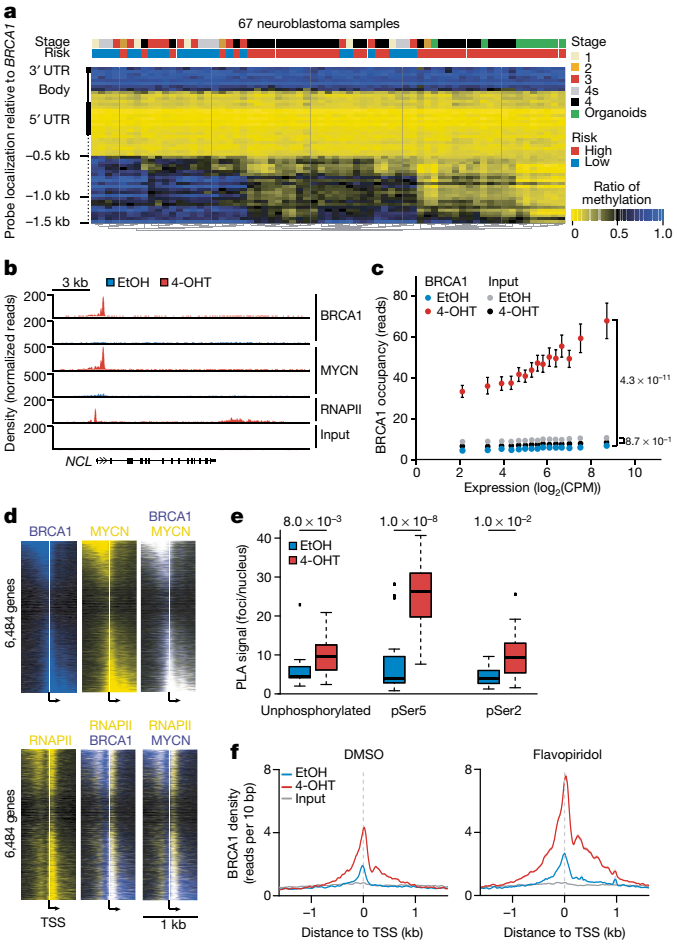

Fig. 2 | Status of BRCA1 in *MYCN*-amplified neuroblastoma cells and its MYCN-dependent recruitment to chromatin. a, *BRCA1* genomic region with average methylation status of 67 primary neuroblastomas and organoids. UTR, untranslated region. **b**, Genome browser tracks of the *NCL* locus after 3 h (RNAPII and MYCN) and 5 h (BRCA1) treatment with 4-OHT. $n = 2$. **c**, BRCA1 occupancy in promoter-proximal regions. In total, 7,812 expressed genes ($\log_2$(CPM) > 1.28; CPM, counts per million) with a BRCA1 peak in the promoter were binned. Data are mean ± 95% confidence interval. *P* values for the difference in slopes between without 4-OHT and with 4-OHT were calculated using a linear model and analysis of covariance (ANCOVA). **d**, Position of BRCA1, MYCN and RNAPII on chromatin relative to the transcription start site. The heat map is sorted by the position of the MYCN-binding site. **e**, Quantification of proximity ligation assays (PLAs) that shows complex formation of BRCA1 with unphosphorylated, and Ser5- and Ser2-phosphorylated RNAPII upon activation of MYCN–ER (4 h). *P* values were calculated using a two-tailed Wilcoxon rank-sum test ($n = 3$). In the box plot, the central line reflects the median and the borders of the boxes show the interquartile range of the plotted data. The whiskers extend to 1.5× the interquartile range and outliers are shown as dots. **f**, BRCA1 occupancy after treatment with 4-OHT or ethanol (5 h) in DMSO-treated (top) and flavopiridol-treated (bottom) cells. Data are mean ± s.e.m.

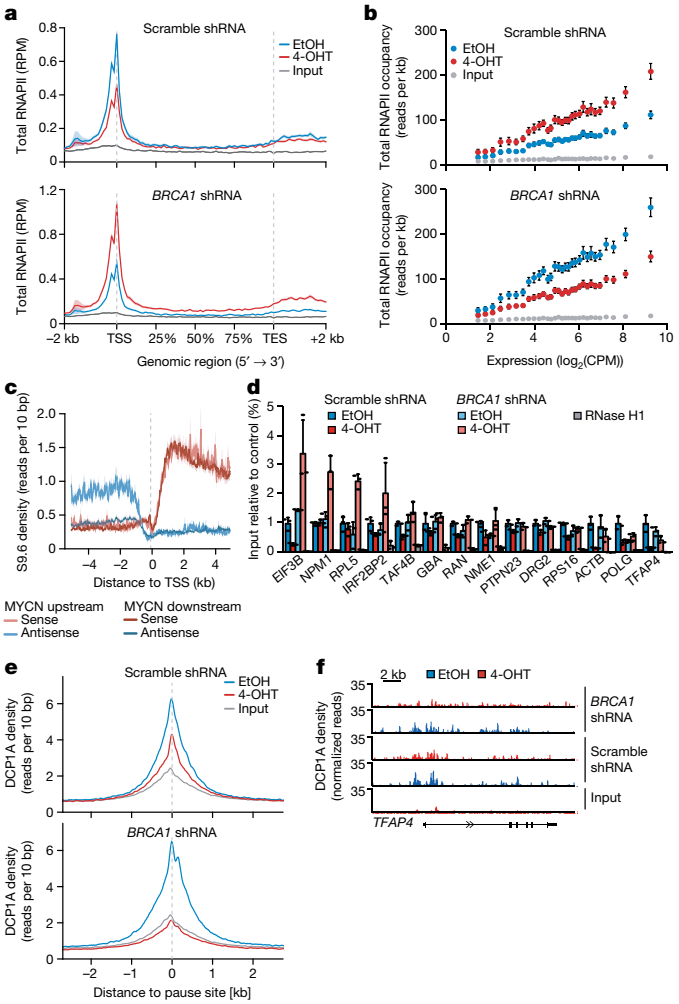

Fig. 3 | BRCA1 is required for MYCN-dependent elongation by RNAPII. a, Metagene plots of total RNAPII after 4-OHT treatment (3 h) in control and *BRCA1*-depleted cells treated with *BRCA1* shRNA 2 for 914 MYCN-activated genes ($n = 2$). Data are mean ± s.e.m. **b**, Correlation between gene expression ($n = 3$) and RNAPII occupancy at promoters in control and *BRCA1*-depleted cells treated with *BRCA1* shRNA 2. Genes were grouped into 30 bins (300 genes per bin) and the mean for each bin is plotted with 95% confidence interval. **c**, Strand-specific DNA–RNA immunoprecipitation coupled to high-throughput sequencing data stratified by position of the MYCN-binding site. **d**, DNA–RNA immunoprecipitation documenting R-loops at the indicated loci upon depletion of *BRCA1* and activation of MYCN (4 h). Data are normalized to control (scramble shRNA, ethanol). Data are mean ±s.d. of technical triplicates. $n = 4$. **e**, Density plot of DCP1A occupancy after 4-OHT treatment (5 h) in control or *BRCA1*-depleted cells treated with *BRCA1* shRNA 2. Data are mean ± s.e.m. **f**, Genome browser tracks of the *TFAP4* locus show chromatin association of DCP1A in cells treated as in **e**.

localized 5′ of the transcription start site often display an R-loop on the antisense strand, whereas this is not observed if the MYCN–BRCA1 site is localized 3′ of the transcription start site (Fig. 3c), which suggests that there is selective pressure for the presence of a MYCN-binding site in the immediate vicinity of an R-loop. We chose 22 R-loop-containing promoters and validated the presence of an R-loop on 14 of them by DNA–RNA immunoprecipitation using the well-characterized R-loops in the *ACTB* gene as positive control[14] (Fig. 3d and Extended Data Fig. 8a, b). On 13 out of 14 of these, activation of MYCN suppressed R-loop formation in control cells. In *BRCA1*-depleted cells, MYCN-dependent R-loop suppression was strongly compromised on all promoters and activation of MYCN enhanced R-loop formation on 8 out of 14 promoters.

BRCA1 promotes R-loop resolution at transcription end sites by recruiting senataxin, an R-loop-specific DNA/RNA helicase[14]. However, depletion of *BRCA1* enhanced senataxin binding to promoter-proximal regions (Extended Data Fig. 8c). Two termination pathways can limit promoter-proximal accumulation of RNAPII: mRNA decapping, which occurs at the pause site[16], and promoter-proximal poly-adenylation[17]. Upon *BRCA1* depletion, activation of MYCN promotes RNAPII accumulation at the pause site, upstream of the most 5′-located polyadenylation site (Extended Data Fig. 8d). Global run-on sequencing showed a drop in nascent transcription close to the pause site (Extended Data Fig. 8e). BRCA1 binds to EDC4, an assembly factor for mRNA decapping complexes[18]. ChIP–seq of DCP1A,

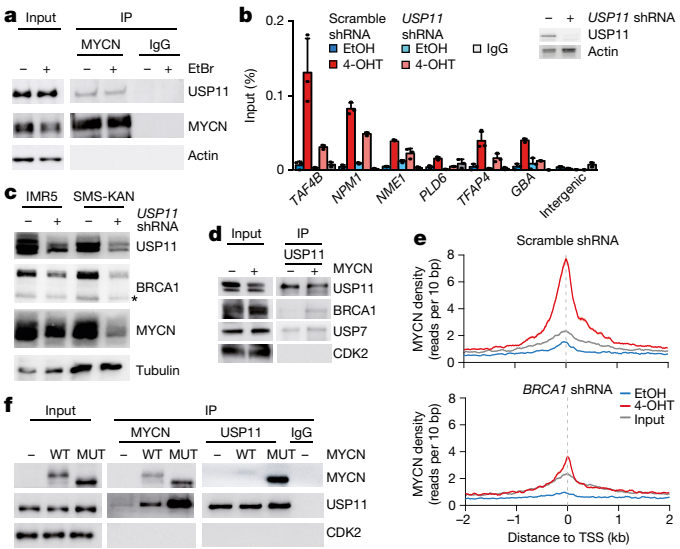

Fig. 4 | MYCN, USP11 and BRCA1 stabilize each other on chromatin. **a**, Immunoblot of anti-MYCN immunoprecipitates (IP) from *MYCN*-amplified (IMR32) neuroblastoma cells. Where indicated, ethidium bromide (EtBr) (1 mg ml^{-1}) was added to the lysate to disrupt DNA-mediated interactions. The input corresponds to 1% of the total protein amount. $n = 3$. **b**, Left, ChIP of BRCA1 in SH-EP MYCN–ER cells that express either scramble shRNA or *USP11* shRNA upon 4-OHT treatment (5 h). Data are mean + s.d. of technical triplicates. $n = 2$. Right, immunoblot of cells used for the ChIP experiment. Actin is used as loading control. $n = 2$. **c**, Immunoblots of indicated proteins after knockdown of *USP11* in *MYCN*-amplified neuroblastoma cells. Asterisk denotes an unspecific band. Tubulin is used as loading control. $n = 3$. **d**, Immunoblots of anti-USP11 immunoprecipitates from control cells or cells that express constitutively active MYCN. CDK2 is used as loading control. The input corresponds to 2% of the total protein amount. $n = 2$. **e**, Density plot of MYCN occupancy after 4-OHT treatment (3 h) in control (top) or *BRCA1*-depleted (bottom) cells treated with *BRCA1* shRNA 2 around transcription start sites. **f**, Immunoblots of anti-USP11 and anti-MYCN immunoprecipitates from SH-EP cells that stably express wild-type (WT) MYCN or MYCN(T58A/S62A) (MUT), as indicated. CDK2 is used as loading control. The input corresponds to 1% of the total protein amount. $n = 3$.

which forms catalytically active decapping complexes with DCP2 upon EDC4-mediated assembly[19], showed that depletion of *BRCA1* had no effect on the association of DCP1A with chromatin in control cells. Activation of MYCN led to a moderate decrease in DCP1A–chromatin association in control cells, but to a complete loss of DCP1A from promoter-proximal regions in *BRCA1*-depleted cells, which indicates that recruitment of BRCA1 by MYCN enables mRNA decapping when RNAPII stalls (Fig. 3e, f).

Proteomic analyses did not show an interaction between BRCA1 and MYCN, which suggests that BRCA1 recruitment is indirect[20]. BRCA1 can be recruited to chromatin by the ubiquitin-specific protease USP11 in a cell-cycle-dependent manner[21]. MYCN recruited BRCA1 to promoter-proximal regions during S and G2 phases, but not in G1 (Extended Data Fig. 9a), and the association between MYCN and BRCA1 followed a similar regulation (Extended Data Fig. 9b–d). USP11 is present in MYCN complexes[20] (Fig. 4a). USP11 heterodimerizes with USP7[22], which also associates with MYCN[23] (Extended Data Fig. 9e). shRNA-mediated depletion showed that USP11 promotes MYCN-dependent recruitment of BRCA1 (Fig. 4b). Indeed, depletion of *USP11* strongly reduced expression of both BRCA1 and MYCN (Fig. 4c), arguing that USP11 stabilizes MYCN–BRCA1 complexes. Incubation with the proteasome inhibitor MG-132 reverted the decrease in MYCN levels and partially reverted the decrease in BRCA1 levels in response to *USP11* depletion, which suggests that the deubiquitinating activity of USP11 contributes to the stabilization of MYCN and BRCA1 (Extended Data Fig. 9f). Conversely, MYCN promoted complex formation of endogenous USP11 with BRCA1 (Fig. 4d). Consistent with the observation that USP11 stabilizes MYCN, depletion of *BRCA1* reduced the association of with MYCN (Fig. 4e). The data show that USP11, MYCN and BRCA1 form a stable complex in neuroblastoma cells.

Pause release of RNAPII by MYC requires the proteasomal turnover of MYC[24], which suggests that the turnover of MYCN limits accumulation of the MYCN–BRCA1–USP11 complex. Turnover of MYCN is controlled by phosphorylation of two residues, Ser62 and Thr58, in a highly conserved domain called MYCBoxI; phosphorylated Thr58 is recognized by the FBXW7 ubiquitin ligase, which targets MYCN for degradation[25]. Alternatively, Thr58 can be dephosphorylated by EYA phosphatases, preventing FBXW7-dependent turnover[26]. Mass spectrometry demonstrated that all four possible phosphorylated forms—including MYCN that is unphosphorylated or monophosphorylated at Ser62—are present in neuroblastoma cells (Extended Data Fig. 9g). Binding of USP11 to MYCN was enhanced by a Thr58/Ser62 double alanine substitution (Fig. 4f) and by individual substitutions of Ser62 and Thr58 (Extended Data Fig. 9h). Because phosphorylation at Ser62 primes phosphorylation at Thr58 by GSK3, the S62A-mutated allele of MYCN shows reduced phosphorylation at Thr58, but not vice versa (Extended Data Fig. 9i). The data show that dephosphorylation of MYCN at Thr58 is critical for binding of USP11; consistently, proteasomal turnover of MYCN limited the accumulation of MYCN–BRCA1 complexes (Extended Data Fig. 9j).

BRCA1 is part of the cellular stress response, which suggests that transcription-induced stress contributes to BRCA1 recruitment. Inhibition of ATR using VE-821 had no effect on the recruitment of BRCA1, and suppressed phosphorylation of CHK1 at Ser345 (Extended Data Fig. 10a, b). MYCN interacts with poly-ADP-ribose polymerase (PARP1), and PARP1 regulates BRCA1 function in homologous recombination[20,27]. However, inhibition of PARP1 had no effect on BRCA1 recruitment (Extended Data Fig. 10c). Together with the observation that BRCA1 is not recruited only in S phase, these findings indicate that replication–transcription conflicts are not the major cause for BRCA1 recruitment. Transcriptional activation induces torsional stress[28]. MYCN interacts with TOPO2A and may relieve torsional stress at promoters[20]. Indeed, inhibition of type II topoisomerases induced BRCA1 accumulation downstream of active promoters and activation of MYCN enhanced recruitment (Extended Data Fig. 10d, e).

MYC was able to bind USP11, but was unable to promote association of USP11 with BRCA1 (Extended Data Fig. 10f). MYCN was more efficient than MYC in recruiting BRCA1 to chromatin (Extended Data Fig. 10g). MYC and MYCN differ in their response to transcriptional stress because MYC, in contrast to MYCN, is able to recruit MIZ1 to buffer excessive transcriptional activation[29]. We hypothesize that MYC and MYCN engage different mechanisms of coping with deregulated transcriptional elongation and that *MYCN*-amplified neuroblastoma tumours are characterized by the ability of MYCN to engage an USP11–BRCA1-dependent pathway that suppresses the accumulation of stalled RNAPII (Extended Data Fig. 10h).

Online content

Any methods, additional references, Nature Research reporting summaries, source data, statements of data availability and associated accession codes are available at https://doi.org/10.1038/s41586-019-1030-9.

Received: 1 May 2018; Accepted: 18 February 2019;
Published online 20 March 2019.

1. Rickman, D. S., Schulte, J. H. & Eilers, M. The expanding world of N-MYC-driven tumors. *Cancer Discov.* **8**, 150–163 (2018).
2. Nie, Z. et al. c-Myc is a universal amplifier of expressed genes in lymphocytes and embryonic stem cells. *Cell* **151**, 68–79 (2012).
3. Rahl, P. B. et al. c-Myc regulates transcriptional pause release. *Cell* **141**, 432–445 (2010).
4. Pao, G. M. et al. Role of BRCA1 in brain development. *Proc. Natl Acad. Sci. USA* **111**, E1240–E1248 (2014).
5. Kortlever, R. M. et al. Myc cooperates with Ras by programming inflammation and immune suppression. *Cell* **171**, 1301–1315 (2017).

6. de Pretis, S. et al. Integrative analysis of RNA polymerase II and transcriptional dynamics upon MYC activation. *Genome Res.* **27**, 1658–1664 (2017).
7. Lorenzin, F. et al. Different promoter affinities account for specificity in MYC-dependent gene regulation. *eLife* **5**, e15161 (2016).
8. Muhar, M. et al. SLAM-seq defines direct gene-regulatory functions of the BRD4–MYC axis. *Science* **360**, 800–805 (2018).
9. Ginno, P. A., Lim, Y. W., Lott, P. L., Korf, I. & Chédin, F. GC skew at the 5′ and 3′ ends of human genes links R-loop formation to epigenetic regulation and transcription termination. *Genome Res.* **23**, 1590–1600 (2013).
10. Quinet, A., Lemaçon, D. & Vindigni, A. Replication fork reversal: players and guardians. *Mol. Cell* **68**, 830–833 (2017).
11. Gorthi, A. et al. EWS–FLI1 increases transcription to cause R-loops and block BRCA1 repair in Ewing sarcoma. *Nature* **555**, 387–391 (2018).
12. Scully, R. et al. BRCA1 is a component of the RNA polymerase II holoenzyme. *Proc. Natl Acad. Sci. USA* **94**, 5605–5610 (1997).
13. Zhang, X. et al. Attenuation of RNA polymerase II pausing mitigates BRCA1-associated R-loop accumulation and tumorigenesis. *Nat. Commun.* **8**, 15908 (2017).
14. Hatchi, E. et al. BRCA1 recruitment to transcriptional pause sites is required for R-loop-driven DNA damage repair. *Mol. Cell* **57**, 636–647 (2015).
15. Chen, L. et al. R-ChIP using inactive RNase H reveals dynamic coupling of R-loops with transcriptional pausing at gene promoters. *Mol. Cell* **68**, 745–757 (2017).
16. Brannan, K. et al. mRNA decapping factors and the exonuclease Xrn2 function in widespread premature termination of RNA polymerase II transcription. *Mol. Cell* **46**, 311–324 (2012).
17. Almada, A. E., Wu, X., Kriz, A. J., Burge, C. B. & Sharp, P. A. Promoter directionality is controlled by U1 snRNP and polyadenylation signals. *Nature* **499**, 360–363 (2013).
18. Hernández, G. et al. Decapping protein EDC4 regulates DNA repair and phenocopies BRCA1. *Nat. Commun.* **9**, 967 (2018).
19. Chang, C. T., Bercovich, N., Loh, B., Jonas, S. & Izaurralde, E. The activation of the decapping enzyme DCP2 by DCP1 occurs on the EDC4 scaffold and involves a conserved loop in DCP1. *Nucleic Acids Res.* **42**, 5217–5233 (2014).
20. Büchel, G. et al. Association with Aurora-A controls N-MYC-dependent promoter escape and pause release of RNA polymerase II during the cell cycle. *Cell Rep.* **21**, 3483–3497 (2017).
21. Orthwein, A. et al. A mechanism for the suppression of homologous recombination in G1 cells. *Nature* **528**, 422–426 (2015).
22. Maertens, G. N., El Messaoudi-Aubert, S., Elderkin, S., Hiom, K. & Peters, G. Ubiquitin-specific proteases 7 and 11 modulate Polycomb regulation of the INK4a tumour suppressor. *EMBO J.* **29**, 2553–2565 (2010).
23. Tavana, O. et al. HAUSP deubiquitinates and stabilizes N-Myc in neuroblastoma. *Nat. Med.* **22**, 1180–1186 (2016).
24. Jaenicke, L. A. et al. Ubiquitin-dependent turnover of MYC antagonizes MYC/PAF1C complex accumulation to drive transcriptional elongation. *Mol. Cell* **61**, 54–67 (2016).
25. Farrell, A. S. & Sears, R. C. MYC degradation. *Cold Spring Harb. Perspect. Med.* **4**, a014365 (2014).
26. Li, J. et al. EYA1's conformation specificity in dephosphorylating phosphothreonine in Myc and its activity on Myc stabilization in breast cancer. *Mol. Cell. Biol.* **37**, e00499-16 (2016).
27. Hu, Y. et al. PARP1-driven poly-ADP-ribosylation regulates BRCA1 function in homologous recombination-mediated DNA repair. *Cancer Discov.* **4**, 1430–1447 (2014).
28. Kouzine, F. et al. Transcription-dependent dynamic supercoiling is a short-range genomic force. *Nat. Struct. Mol. Biol.* **20**, 396–403 (2013).
29. Vo, B. T. et al. The interaction of Myc with Miz1 defines medulloblastoma subgroup identity. *Cancer Cell* **29**, 5–16 (2016).

Acknowledgements This work was supported by grants from the European Research council (AuroMYC), the German Cancer Aid (111300), the Federal Ministry of Education and Research (SYSMED) and the German Research Foundation (WO 2108/1-1). We thank J. Dirks and M. Brockmann for initial experiments on USP11.

Reviewer information *Nature* thanks Bruno Amati, Ashok Venkitaraman and the other anonymous reviewer(s) for their contribution to the peer review of this work.

Author contributions S.H., J. Kalb, G.B. and A.C. performed most experiments, D.S. and C.K. performed PLA assays, S.R. performed replication assays, C.S.-V. performed immunofluorescence experiments. G.B. performed DNA–RNA immunoprecipitation and global run-on sequencing analyses, A.B. performed 4-thiouridine-sequencing analyses, J.X. and C.P.A. performed shRNA screening, S.W. analysed ChIP–seq and RNA-sequencing data, A.B., M.E. and C.P.A. analysed additional high-throughput data, J. Koster analysed methylation status in neuroblastomas, M.D., E.W., J.M., R.V., S.H. and M.E. devised and supervised experiments, and S.H. and M.E. wrote the paper.

Competing interests The authors declare no competing interests.

Additional information

Extended data is available for this paper at https://doi.org/10.1038/s41586-019-1030-9.
Supplementary information is available for this paper at https://doi.org/10.1038/s41586-019-1030-9.
Reprints and permissions information is available at http://www.nature.com/reprints.
Correspondence and requests for materials should be addressed to S.H. or M.E.

METHODS

Detailed information about cell lines, antibodies, reagents, commercial kits, primers, siRNA and shRNA sequences and used software is reported in Supplementary Table 2.

Cell culture. Neuroblastoma cell lines (IMR-32, IMR-5, SH-EP and SMS-KAN) were verified by single tandem repeat profiling and grown in RPMI 1640 (Sigma-Aldrich and Thermo Fisher Scientific). HEK293TN, Plat-E, KPC and NIH-3T3 cells were grown in DMEM (Sigma-Aldrich and Thermo Fisher Scientific). Medium was supplemented with 10% fetal calf serum (Biochrom and Sigma-Aldrich) and penicillin–streptomycin (Sigma-Aldrich). All cells were routinely tested for mycoplasma contamination. Where indicated, cells were treated with 4-OHT (Sigma-Aldrich), flavopiridol (Sigma-Aldrich), THZ1 (Hycultec) or etoposide (Sigma-Aldrich). For double-thymidine block, cells were treated for 16 h with 2 mM thymidine (Sigma-Aldrich), released for 8 h into normal medium and then blocked again (2 mM, 16 h). For release, cells were washed with PBS before medium was added.

For the clonogenic assay, 1×10^5 SH-EP MYCN–ER cells previously infected and selected as described in 'Transfection and lentiviral infection' were plated and treated from the following day onwards with 200 nM 4-OHT or ethanol for 6 days. Fresh medium with 4-OHT or ethanol was added every second day. Cells were fixed with 3.7% formaldehyde for 20 min. After aspirating the medium, crystal violet solution (0.1% crystal violet, 20% ethanol in ddH_2O) was added for overnight staining and cells were washed the next day with ddH_2O.

Transfection and lentiviral infection. Transfection with siRNA was performed using the RNAiMAX reagent according to the manufacturer's protocol. Cells were collected 72 h after transfection. Transfection with cDNA was performed using PEI (Sigma-Aldrich). Cells were collected 48 h after transfection. For lentivirus production, HEK293TN cells were transfected using PEI. Lentivirus expressing shRNA targeting *BRCA1* was produced by transfection with the pGIPZ plasmid together with the packaging plasmid psPAX.2 and the envelope plasmid pMD2.G. Lentivirus expressing shRNA targeting *USP11* was produced by transfection with the pLKO plasmid. Virus-containing supernatant was collected 48 h and 72 h after transfection. SH-EP cells were infected with lentiviral supernatants in the presence of 4 $\mu g\ ml^{-1}$ polybrene for 24 h. Cells were selected for 2 days with puromycin (2 $\mu g\ ml^{-1}$; IMR5 0.5 $\mu g\ ml^{-1}$) and afterwards plated for the experiment.

Immunoblot and immunoprecipitation. Whole-cell extracts were prepared using NP-40 buffer (50 mM Tris (pH 8.0), 150 mM NaCl, 1% NP-40) with three rounds of freeze–thaw cycles or RIPA buffer (50 mM HEPES, 140 mM NaCl, 1 mM EDTA, 1% triton X-100, 0.1% sodium deoxycholate and 0.1% SDS) containing protease and phosphatase inhibitor cocktails (Sigma-Aldrich). Lysates were cleared by centrifugation, separated on SDS or Bis-Tris gels and transferred to a PVDF membrane (Millipore).

For immunoprecipitation, cells were resuspended in lysis buffer containing 20 mM HEPES-KOH (pH 7.8), 140 mM KCl, 0.2 mM EDTA, 0.1% NP-40 supplemented with a cocktail of protease and phosphatase inhibitors. After brief sonication, samples were incubated on ice for 30 min and cleared by centrifugation. Co-immunoprecipitation was carried out in lysis buffer using 2 μg of antibodies and 1–2 mg lysate.

For immunoblots showing multiple proteins with similar molecular mass, one representative loading control is shown. As loading control, vinculin, actin, tubulin or CDK2 was used. For gel source data, see Supplementary Fig. 1.

Flow cytometry analysis. Flow cytometry (fluorescence-activated cell sorting, FACS) analysis was performed as previously described[30]. Subconfluent cells were labelled with 20 μM BrdU (Sigma-Aldrich) for 1 h. Cells were collected, washed with ice-cold PBS and fixed in 80% ethanol overnight at −20 °C. Cells were washed with cold PBS and incubated in 2 M HCl/0.5% triton X-100 for 30 min at room temperature. Cell pellets were neutralized by incubating with $Na_2B_4O_7$. The pellet was incubated with anti-BrdU–FITC antibody (BioLegend) diluted in 100 μl 1% BSA and 0.5% Tween-20 in PBS for 30 min at room temperature in the dark. After washing with PBS, the cells were resuspended in PBS with RNase A (24 $\mu g\ ml^{-1}$) and propidium iodide (54 μM) and incubated for 30 min at 37 °C.

For FACS using propidium iodide, cells were collected by trypsinization, washed with cold PBS and fixed in 80% ethanol overnight at −20 °C. After washing with PBS, the cells were resuspended in PBS with RNase A (24 $\mu g\ ml^{-1}$) and propidium iodide (54 μM), and incubated for 30 min at 37 °C.

For FACS using annexin V and propidium iodide, the supernatant of the respective cultures was combined with cells collected by trypsinization and washed with cold PBS. Cell pellets were resuspended in 100 μl 1× annexin V-binding buffer (10 mM HEPES pH 7.4, 140 mM NaCl and 2.5 mM $CaCl_2$) and 2 μl annexin V/Pacific Blue dye and incubated for 15 min at room temperature in the dark. Afterwards, 400 μl 1× binding buffer and propidium iodide (54 μM) were added and the samples were stored cold and dark until analysis.

Subsequent analysis of all FACS experiments was performed on a BD FACSCanto II flow cytometer using BD FACSDIVA Software.

DNA–RNA immunoprecipitation. DNA–RNA immunoprecipitation (DRIP) was performed as previously described[31]. In brief, cells were digested with 0.5% SDS and proteinase K overnight. DNA was extracted with phenol/chloroform and precipitated with ethanol. DNA was digested using a cocktail of restriction enzymes (Bsrg1, EcoR1, HindIII, SspI and XbaI) overnight at 37 °C. For RNase H-treated samples, DNA was additionally incubated with RNase H overnight. DNA was purified as described above. S9.6 antibody, which detects RNA–DNA hybrids[32], was coupled to A/G-Dynabeads (Invitrogen). DNA in 1× binding buffer (10 mM $NaPO_4$ pH 7.0, 140 mM NaCl and 0.05% triton X-100) was added to the antibody-coupled beads overnight. After extensive washing, DNA was eluted with elution buffer (50 mM Tris-HCl pH 8.0, 10 mM EDTA and 0.5% SDS) and treated for 2 h at 45 °C with proteinase K. After DNA extraction, locus-specific DRIP signals were assessed by qPCR.

High-throughput sequencing. ChIP and ChIP–seq analyses were performed as previously described[33]. For spike-in experiments (ChIP-Rx), 10% of fixed NIH-3T3 or KPC mouse cell lines were added before lysis. Cells were treated with 1% formaldehyde for 10 min at room temperature following 5 min of incubation with glycine. After cell lysis (5 mM PIPES pH 8.8, 5 mM KCl and 0.5% NP40), nuclei were resuspended in RIPA buffer (50 mM HEPES pH 7.9, 140 mM NaCl, 1% triton X-100, 0.1% deoxycholate, 0.1% SDS and 1 mM EDTA containing protease and phosphatase inhibitor cocktails) and DNA was fragmented to a size of <500 bp using a Branson sonifier. Antibodies were bound to protein A/G-Dynabeads (Invitrogen) and immunoprecipitated. After extensive washing, chromatin was eluted with 1% SDS and crosslinking was reverted overnight. Phenol/chloroform extraction was used for DNA purification. After DNA extraction occupancy of different proteins was assessed by qPCR. qPCR analyses show mean ± s.d. of technical triplicates as well as an overlay of each data point to indicate the distribution of the data.

ChIP–seq was performed as previously described[34]. Purified DNA was end-repaired, A-tailed, ligated to Illumina adaptors, size-selected (200 bp) and purified with a gel-extraction kit. DNA fragments were amplified by 15–18 cycles of PCR, and the library size and amount of library were specified with the Biorad Experion Automated Electrophoresis system or Fragment Analyzer (Advanced Analytical). The library was subjected to Illumina GAIIx or Illumina NextSeq 500 sequencing, according to the manufacturer's instructions. After base-calling using the CASAVA software (GAIIx sequencing) or Illumina's FASTQ Generation software v.1.0.0 (NextSeq 500 sequencing), high quality PF-clusters were selected for further analysis.

RNA sequencing was performed as previously described[24] using an Illumina NextSeq 500. RNA was extracted using RNeasy mini columns (Qiagen) including on-column DNase I digestion. mRNA was isolated using the NEBNext Poly(A) mRNA Magnetic Isolation Module (NEB) and library preparation was performed with the NEBNext Ultra RNA Library Prep Kit for Illumina following the instruction manual. Libraries were size-selected using Agencourt AMPure XP Beads (Beckman Coulter) followed by amplification with 12 PCR cycles. Library quantification and size determination was performed with the Biorad Experion Automated Electrophoresis system or Fragment Analyzer (Advanced Analytical).

For 4-thiouridine (4sU)-labelled nascent RNA sequencing, SH-EP MYCN–ER cells were cultured at a density of 5 million cells per plate 24 h before treatment with 4-OHT. Before collection of RNA using the Qiagen miRNeasy kit, nascent RNA was labelled by adding 200 μM of 4sU (Sigma-Aldrich) in RPMI medium to the cells for 15 min under normal culture conditions. After extraction and quantification of total RNA by Nanodrop, equal amounts were labelled with biotin (Pierce) in the presence of DMF–HPDP buffer. Free biotin removal was carried out by chloroform–isoamyl alcohol extraction, after which RNA was resuspended into nuclease free water. Dynabeads MyOne Streptavidin T1 beads (Life Technologies) were used for enrichment of biotinylated RNA, which was then eluted by 100 mM DTT and cleaned by RNeasy MinElute cleanup kit. The nascent RNA concentration was then measured using a RiboGreen RNA assay kit and equal amounts were used for library preparation. Before library preparation, rRNA was depleted using a NEB rRNA depletion kit and then all eluted material was processed using the NEB Ultra Directional kit with 17 PCR cycles. The libraries were then sequenced for 75 cycles using an Illumina NextSeq 500 system.

Global run-on followed by next-generation sequencing (GRO–seq) was carried out as previously described, with a few modifications[35]. In brief, cells were washed twice with cold 1× PBS and collected in 1× PBS. Cells were resuspended in 10 ml swelling buffer (10 mM Tris-HCl pH 7.5, 2 mM $MgCl_2$ and 3 mM $CaCl_2$) and incubated for 5 min on ice. After centrifugation (400*g*, 10 min), cells were resuspended in 10 ml swelling buffer containing 10% glycerol. Then, 10 ml lysis buffer (10 mM Tris-HCl pH 7.5, 2 mM $MgCl_2$, 3 mM $CaCl_2$, 10% glycerol and 1% Igepal) was added with gently swirling and the sample was incubated for 5 min on ice. The volume of cell suspension was brought to 45 ml with lysis buffer. Resultant nuclei were washed with 10 ml freezing buffer (40% glycerol, 50 mM Tris-HCl pH 8.0, 5 mM $MgCl_2$ and 0.1 mM EDTA). The pellet was resuspended in 100 μl freezing buffer per 1×10^7 of nuclei.

For run-on reactions, resuspended nuclei were mixed with the same amount of run-on reaction buffer (10 mM Tris-HCl pH 8.0, 5 mM $MgCl_2$, 300 mM KCl, 1 mM DTT, 500 μM ATP, 500 μM GTP, 500 μM Br-UTP, 2 μM CTP, 200 U ml^{-1} Superase In and 1% *N*-laurylsarcosine) and incubated 7 min at 30 °C. The reaction was blocked by adding 600 μl Trifast, thoroughly vortexing and incubating for 5 min. RNA was extracted by adding 160 μl chloroform, precipitated with ethanol and resuspended in 20 μl H_2O. RNA was next subjected to DNase treatment (Turbo DNA-free kit, Thermo Fisher) twice according to manufacturer's protocol. RNA was fragmented using an Ambion RNA fragmentation kit and end-repaired by T4 PNK (NEB).

Anti-BrdU agarose beads (Santa-Cruz, 50 μl per sample) were washed twice and then blocked for 1 h with blocking buffer (1× binding buffer, 0.1% polyvinylpyrrolidone and 0.1% BSA). Beads were washed twice with binding buffer (0.25× SSPE, 0.05% Tween20, 37.5 mM NaCl and 1 mM EDTA) and mixed with RNA in 700 μl binding buffer for 1 h on a rotating wheel. After binding, beads were washed twice with binding buffer, twice with low-salt wash buffer (0.2× SSPE, 0.05% Tween20 and 1 mM EDTA), one time with high-salt wash buffer (0.2× SSPE, 137.5 mM NaCl, 0.05% Tween20 and 1 mM EDTA) and twice with TE with 0.05% Tween20. Finally, RNA was eluted four times with 100 μl elution buffer (50 mM Tris pH 7.5, 150 mM NaCl, 0.1% SDS, 20 mM DTT and 1 mM EDTA) at 37 °C. RNA was purified with TRIzol and chloroform as described above. RNA was decapped using RppH (NEB) with 10× NEB Thermopol buffer for 1 h at 37 °C. Reactions were stopped by adding EDTA and incubation at 65 °C for 5 min. Afterwards RNA was extracted as described above. Library preparation was done according to the manufacturer's instructions using a NEBNext Multiplex Small RNA Library Prep Kit for Illumina.

shRNA screening. A total of 18,290 shRNAs of the Open Biosystems (Dharmacon; GE Lifesciences) pGIPZ shRNA library (releases 6.1–6.12) were screened in two pools (consisting of 9,589 and 8,701 individual shRNAs) and each pool in two independent biological replicates. Upon reannotation using the human transcriptome hg19 (Homo_sapiens.GRCh37.74.cDNA.all.fa), 12,931 shRNAs were found to target 9,601 genes. Of these, 1, 8, 10, 96, 429, 2,098 and 6,959 were targeted with 7, 6, 5, 4, 3, 2 or 1 individual shRNAs, respectively. Following lentiviral packaging of the plasmids, SH-EP MYCN–ER cells were transduced with the viral library at a multiplicity of infection of 0.1. Infected cells were selected with puromycin for three days and the screen was started immediately after selection was completed. Cells were collected before the treatment with ethanol or 4-OHT (condition 'start') and after two weeks of treatment with either ethanol (control) or 4-OHT (activation of MYCN). Cell numbers were counted regularly over the entire course of the screening experiment to verify an equal number of population doublings in both conditions. Every 2–3 days, the cells of both conditions were split and supplied with fresh 4-OHT or ethanol. The number of cells was always kept at a minimum of 1.0×10^7 cells to guarantee a sufficient minimum representation of all shRNAs. Genomic DNA was isolated using DNAzol (Invitrogen) followed by ethanol precipitation. shRNA hairpin sequences were recovered from the genomic host cell DNA in an amplification reaction using custom PCR primers that specifically bind to the pGIPZ vector sequences that flank the shRNA sequences. For each condition, 70 identical PCRs of 24 cycles and with 1 μg of genomic DNA each were carried out and corresponding products were pooled and gel-purified. The quantity and size of the purified PCR products was determined using the Experion Automated Electrophoresis System (Bio-Rad). Sample-specific DNA libraries were subjected to Illumina GAIIx single-read sequencing according to the manufacturer's instructions. Mapping of the sample-specific reads and initial bioinformatics analyses were done as described in 'Bioinformatics analysis and statistics'. Using *Z*-score statistics for the effect strengths, we identified 104 shRNAs targeting 99 genes that were strongly depleted upon growth of SH-EP MYCN–ER cells in the presence of 4-OHT, but much less depleted in the absence of 4-OHT.

In situ PLA. PLA was performed using the Duolink In situ Kit (Sigma-Aldrich) according to the manufacturer's protocol. For counterstaining of nuclei and actin, Hoechst 33342 (Sigma-Aldrich) and Alexa Fluor 568–phalloidin (Thermo Fisher Scientific), respectively, were used. Images were taken with a confocal microscope (Nikon Ti-Eclipse) with 60× magnification and on an Operetta High-Content Imaging System with 40× magnification. For quantification, not less than 300 cells were analysed using ImageJ (W. Rasband, NIH). Images from Operetta were analysed using Harmony High Content Imaging and Analysis Software. *P* values were calculated using a two-tailed Wilcoxon rank-sum test.

DNA fibre assay. DNA fibre assays to analyse replication fork progression and origin firing were essentially carried out as previously described[36]. Cells were first incubated with 4-OHT for 6 h and afterwards with 5-chloro-2-deoxyuridine (CldU, 25 μM) for 20 min, followed by 5-iodo-2-deoxyuridine (IdU, 25 μM; both from Sigma-Aldrich) for 1 h. DNA fibres were spread on glass slides. After acid treatment, CldU- and IdU-labelled tracts were detected by 1 h incubation at 20 °C with rat anti-BrdU antibody (dilution 1:400 detects BrdU and CldU; AbD Serotec) and mouse anti-BrdU antibody (1:150, detects BrdU and IdU; Becton Dickinson). Slides were fixed in 4% paraformaldehyde in PBS and incubated for 2 h at 20 °C with an Alexa Fluor 555-conjugated goat anti-rat antibody (dilution 1:150) or Alexa Fluor 488-conjugated goat anti-mouse antibody (dilution 1:150; both from Molecular Probes/Thermofisher). Fibre images were acquired by fluorescence microscopy using the Axio Scope A1 running with the microscope software ZEN (both from Zeiss) for image acquisition and processing. For analysis of fibre images, the imaging software ImageJ was used. Statistical analysis of replication fork progression was performed using the two-tailed, unpaired *t*-test with additional Welch's correction in GraphPad Prism v.5.0, because of unequal variances between samples.

Immunofluorescence staining. Cells were infected and selected by puromycin treatment as previously described. After selection, cells were plated in a 96-well plate and incubated with ethanol or 4-OHT from the following day onwards for 24 h (200 nM). The last two hours, etoposide was added as positive control (25 μM). Cells were fixed with 3.7% paraformaldehyde in PBS. After removing paraformaldehyde and washing, cells were permeabilized with 0.2% triton X-100 in PBS and blocked with 3% BSA in PBS. Samples were stained with primary antibodies against γH2A.X (1:400) and 53BP1 (1:500) in 3% BSA in PBS overnight at 4 °C and after washing incubated with secondary antibody (1:400) for 1 h at room temperature. Images were taken with an Operetta High-Content Imaging System with 20× magnification. Images were analysed using Harmony High Content Imaging and Analysis Software.

Bioinformatics analysis and statistics. Base-calling was performed using Illumina's FASTQ Generation software v.1.0.0 and sequencing quality was tested using the FastQC script.

For ChIP–seq, reads were mapped to hg19 using Bowtie1[37] with default parameters, and samples were normalized to the number of mapped reads in the smallest sample. Peak-calling for BRCA1, MYCN and total RNAPII with MACS14[38] was performed with the corresponding input sample as control and with variable settings for duplicates (--keep-dup; (antibody/biological condition/value): BRCA1 ± 4-OHT: 5; BRCA1 ± 4-OHT, ±flavopiridol, ±etoposide: 3; MYCN ± 4-OHT: 5; DCP1A ± 4-OHT, ±*BRCA1* shRNA: 1; MYCN pRRL–MYCN: 1; BRCA1 pWZL–MYCN/pWZL–empty: 5; total RNAPII ethanol: 5) and *P* value (--pvalue; (antibody/biological condition/value): BRCA1 ± 4-OHT: 1×10^{-6}; BRCA1 ± 4-OHT, ±flavopiridol, ±etoposide: 1×10^{-7}; MYCN ± 4-OHT: 1×10^{-11}; DCP1A ± 4-OHT, ±*BRCA1* shRNA: 1×10^{-6}; MYCN pRRL–MYCN: 1×10^{-9}; BRCA1 pWZL–MYCN/pWZL–empty: 1×10^{-9}; total-RNAPII ethanol: 1×10^{-14}). Bedgraph files were generated using the genomecov function from BEDtools[39] and the Integrated Genome Browser[40] was used to visualize these density files. Annotation of peaks to the next RefSeq gene was done with BEDtools closestBed and a promoter was defined as a region ±1 kb relative to the transcription start site (TSS). Read density graphs were obtained using the computeMatrix function from DeepTools[41] at a resolution of 10 bp. For de novo motif analysis the DREME algorithm implemented in the MEME suite[42] was used with default settings and similarities between identified motifs and known motifs were examined with TOMTOM and three databases ('JASPAR Core vertebrates 2014', 'Jolma 2013' and 'Uniprobe mouse'). Relative motif frequencies of E-boxes were counted with an in-house script and curves were smoothed with a moving window of 50 bp. Travelling ratios for RNAPII ChIP–seq were calculated by counting reads using the BEDtools 'coverage' function (parameter: –F 0.51) around the TSS (−30 to +300 bp), within gene bodies (+300 bp to TES) and at the TES (TES to +1 kb) of Ensembl genes. A pseudocount per kb was added, gene body counts were normalized to the length of the gene and, finally, TSS counts were divided by gene body counts. Metagene window plots were generated with NGStools[43] of the indicated gene group. MYCN-activated and -repressed genes are defined by positive and negative $\log_2$(change in expression), respectively, of genes with Benjamini–Hochberg *q*-values (±4-OHT) less than 0.05, with an expression filter that rejects genes with less than 2 CPM.

Classification of genes with strong, weak or no G/C skew was done with skewR[31] using the human hg19 genome, all expressed genes and the parameters: -z 60 –s hg19.fa -m model/GC_SKEW_1mil.hmm -g UCSC_Main_on_Human_refGene_hg19_TSS_toTES.bed -b UCSC_hg19_CpGislands.bed. Gene expression changes in SH-EP MYCN–ER cells after activation of MYCN of the respective class of genes was plotted as kernel density with a bandwidth of 0.05. *P* values were calculated with a two-tailed Wilcoxon one-sample signed-rank test with $\mu = 0$.

To correlate BRCA1 occupancy in promoter-proximal regions before and after activation of MYCN–ER with gene expression, 7,812 expressed genes ($\log_2$(CPM) > 1.28) with a BRCA1 peak in the promoter (±1 kb relative to the TSS) were grouped into 15 equally sized bins and the mean of BRCA1 occupancy in a region of ±100 bp around the peak summit was plotted, including ±95% confidence interval.

For ChIP-Rx–seq, reads were mapped independently to the human hg19 and mouse mm10 (spike-in) genome and a spike-in normalization factor was calculated

by dividing the number of mapped reads of the spike-in of the smallest sample by the number of mapped reads of the spike-in for each sample. For each sample, this factor was multiplied by the number of reads that map to the human genome and all BAM files for subsequent analysis were adjusted to this read count. Peak-calling of the MYCN ChIP-Rx sample '+4-OHT, −*BRCA1* shRNA' was done with MACS14 (keep-dup: 1, *P* value: 1×10^{-10}) with separate peak-calling for the corresponding input sample using the same parameters as the treated sample. Overlapping peaks in the input were then subtracted from the MYCN ChIP-Rx sample resulting in 692 peaks in promoters of RefSeq genes (±1 kb relative to TSS). Read density plots around these TSS were then drawn with a resolution of 10 bp using the 'computeMatrix' and 'plotProfile' function from DeepTools.

For GRO–seq, reads of all biological conditions (±4-OHT, ±*BRCA1* shRNA) were pooled and the 3′ adaptor was trimmed using Cutadapt[44] keeping at least 30 bp. Untrimmed and trimmed reads passing the filter were then mapped to hg19 using TopHat2[45] and Bowtie2[46], including spliced reads. TSS with a called RNAPII peak (ethanol condition) with a maximum distance of 250 bp to the TSS were used as view point for a heat map drawn with 'computeMatrix' and 'plotHeatmap' from DeepTools at a resolution of 1 bp. The resulting heat map is sorted based on the distance of the TSS to the RNAPII peak and additionally contains read coverage from mRNA-sequencing (sample: 'ethanol') and ChIP–seq (samples: 'total RNAPII (N20) ethanol' and corresponding input).

Raw data from DRIPc–seq[47] were downloaded from GEO (GSE70189, sample GSM1720613), strand-specifically mapped to hg19 with Bowtie1, and the read density around TSSs of genes with either up- or downstream MYCN peaks was calculated with DeepTools. Bidirectional genes and genes with multiple annotated TSSs were removed before the density matrix was calculated and the mean profile was drawn. To identify the number of BRCA1/MYCN-bound genes with R-loops, coordinates of R-loops from DRIP–seq experiments from NT2 (two replicates), K562, E14 and NIH-3T3 cells were obtained from GEO (GSE70189) and converted to hg19 if necessary. A consensus R-loops dataset was generated as defined by (1) overlap by at least 1 bp in all samples, (2) overlap by at least 1 bp in an RNase A-treated sample and (3) not overlapping with an RNase H-treated sample. The resulting R-loops were then annotated to the next TSS, MYCN and BRCA1 peak and filtered as indicated. *P* values were calculated with a permutation test ($n = 10{,}000$).

Coordinates of polyA sites were downloaded from UCSC (UHR; two replicates)[48], extended in both directions by 15 bp and overlapping polyA sites from both replicates were extracted. For each annotated RefSeq TSS, the first downstream intronic polyA site in a region of TSS to +5 kb that is not in a window of ±1 kb around a TES was used to analyse RNAPII density.

For mRNA sequencing, reads were mapped to hg19 using TopHat2[45] and Bowtie2[46] and samples were normalized to the number of mapped reads in the smallest sample. Reads per gene were counted using the 'summarizeOverlaps' function from the R package 'GenomicAlignments' using the 'union' mode and Ensembl genes. Non- and weakly expressed genes were removed (mean count over all samples < 1 (*BRCA1* shRNA experiment) or < 1.28 (MYCN–ER ± 4-OHT; GSE78957)). Differentially expressed genes were called with edgeR and *P* values were adjusted for multiple testing using the Benjamini–Hochberg procedure. Gene set enrichment analyses[49] were done with the 'Hallmark', 'C2' and 'C7' databases from MSigDB[50], 1,000 permutations and default settings. For bin plots, genes were sorted on the basis of the indicated criterion, grouped into equally sized bins and the mean or median was calculated. *P* values for the difference in slopes were calculated using a linear model and analysis of variance (ANOVA). To calculate *P* values comparing the median of different groups in box plots, a two-tailed Wilcoxon signed-rank test (for paired data) or a two-tailed Wilcoxon rank-sum test (unpaired data) was used.

To correlate MYCN-dependent gene expression changes with gene expression in neuroblastoma tumour samples, normalized expression values from GSE62564[51] were downloaded from GEO, row-wise median-centred and the top 400 differentially expressed genes between stage 4 and stage 1/2/3/4s were defined with: $(\text{mean}_{\text{stage4}} - \text{mean}_{\text{stage1,2,3,4s}})/(\text{s.d.}_{\text{stage4}} + \text{s.d.}_{\text{stage1,2,3,4s}})$. For each tumour sample, the Pearson's correlation coefficient between the median-centred expression and the gene expression changes between scramble shRNA 4-OHT versus scramble shRNA ethanol was calculated. Kaplan–Meier survival curves stratified by BRCA1 expression from the same dataset were calculated using the R2: Genomics Analysis and Visualization Platform (http://r2.amc.nl) in 'scanning' mode.

Methylation data from human neuroblastoma tumour samples and corresponding meta information were taken from GSE76269 and the R2 platform was used for visualization of the methylation status of probes within the *BRCA1* genomic locus. The ratio of methylation is defined as signal (methylated)/signal (methylated + unmethylated).

For 4sU-seq, fastq generation, quality check, read mapping, and normalization of mapped reads and differential expression analyses, the analysis was carried out in the same way as for mRNA sequencing, with the difference being that the reads falling in exons were not considered. In total, 18,213 genes were grouped into 39 equally sized bins.

For analysing the shRNA screen, fastq files were mapped to a custom reference database that contains the guide-stem sequences of all screened shRNAs. Mapping was done using Bowtie v.0.12.8, not allowing any mismatches. Mapped reads per sample were counted and combined in one count matrix. Average values of size-normalized counts for corresponding conditions from replicate experiments were used to calculate relevant fold changes to determine enrichment or depletion of individual shRNAs between conditions. A *Z*-score statistic was applied to all calculated $\log_2$(fold change in abundance) (indicating the number of standard deviations an effect is above or below the mean of the overall population of shRNAs), to compare the results from the two separately screened shRNA pools and to determine cut-off values for a combined hit selection. shRNAs with *Z*-scores of $Z < -3$ for the change in abundance between the ethanol-treated and the 4-OHT-treated conditions were defined as 'synthetic lethal hits' as long as the *Z*-score for the change in abundance between the starting condition and the ethanol-treated control condition was $Z > -3$.

In box plots, the central line reflects the median and the borders of the boxes show the interquartile range of the plotted data. The whiskers extend to 1.5× the interquartile range and outliers are shown as dots.

Reporting summary. Further information on research design is available in the Nature Research Reporting Summary linked to this paper.

Data availability

ChIP–seq and mRNA-sequencing datasets as well as results from the shRNA screen are available at the Gene Expression Omnibus (GEO) under accession number GSE111905. 4sU-sequencing data are available at the GEO under the accession number GSE113861.

30. Schülein-Völk, C. et al. Dual regulation of Fbw7 function and oncogenic transformation by Usp28. *Cell Rep.* **9**, 1099–1109 (2014).
31. Ginno, P. A., Lott, P. L., Christensen, H. C., Korf, I. & Chédin, F. R-loop formation is a distinctive characteristic of unmethylated human CpG island promoters. *Mol. Cell* **45**, 814–825 (2012).
32. Boguslawski, S. J. et al. Characterization of monoclonal antibody to DNA·RNA and its application to immunodetection of hybrids. *J. Immunol. Methods* **89**, 123–130 (1986).
33. Walz, S. et al. Activation and repression by oncogenic MYC shape tumour-specific gene expression profiles. *Nature* **511**, 483–487 (2014).
34. Chen, X. et al. Integration of external signaling pathways with the core transcriptional network in embryonic stem cells. *Cell* **133**, 1106–1117 (2008).
35. Gardini, A. Global run-on sequencing (GRO–seq). *Methods Mol. Biol.* **1468**, 111–120 (2017).
36. Klusmann, I. et al. p53 activity results in DNA replication fork processivity. *Cell Rep.* **17**, 1845–1857 (2016).
37. Langmead, B., Trapnell, C., Pop, M. & Salzberg, S. L. Ultrafast and memory-efficient alignment of short DNA sequences to the human genome. *Genome Biol.* **10**, R25 (2009).
38. Zhang, Y. et al. Model-based analysis of ChIP–seq (MACS). *Genome Biol.* **9**, R137 (2008).
39. Quinlan, A. R. & Hall, I. M. BEDTools: a flexible suite of utilities for comparing genomic features. *Bioinformatics* **26**, 841–842 (2010).
40. Freese, N. H., Norris, D. C. & Loraine, A. E. Integrated genome browser: visual analytics platform for genomics. *Bioinformatics* **32**, 2089–2095 (2016).
41. Ramírez, F., Dündar, F., Diehl, S., Grüning, B. A. & Manke, T. deepTools: a flexible platform for exploring deep-sequencing data. *Nucleic Acids Res.* **42**, W187–W191 (2014).
42. Bailey, T. L. et al. MEME SUITE: tools for motif discovery and searching. *Nucleic Acids Res.* **37**, W202–W208 (2009).
43. Shen, L., Shao, N., Liu, X. & Nestler, E. ngs.plot: quick mining and visualization of next-generation sequencing data by integrating genomic databases. *BMC Genomics* **15**, 284 (2014).
44. Martin, M. Cutadapt removes adapter sequences from high-throughput sequencing reads. *EMBnet J* **17**, 10–12 (2011).
45. Kim, D. et al. TopHat2: accurate alignment of transcriptomes in the presence of insertions, deletions and gene fusions. *Genome Biol.* **14**, R36 (2013).
46. Langmead, B. & Salzberg, S. L. Fast gapped-read alignment with Bowtie 2. *Nat. Methods* **9**, 357–359 (2012).
47. Sanz, L. A. et al. Prevalent, dynamic, and conserved R-Loop structures associate with specific epigenomic signatures in mammals. *Mol. Cell* **63**, 167–178 (2016).
48. Derti, A. et al. A quantitative atlas of polyadenylation in five mammals. *Genome Res.* **22**, 1173–1183 (2012).
49. Subramanian, A. et al. Gene set enrichment analysis: a knowledge-based approach for interpreting genome-wide expression profiles. *Proc. Natl Acad. Sci. USA* **102**, 15545–15550 (2005).
50. Liberzon, A. et al. The Molecular Signatures Database (MSigDB) hallmark gene set collection. *Cell Syst.* **1**, 417–425 (2015).
51. Su, Z. et al. An investigation of biomarkers derived from legacy microarray data for their utility in the RNA-seq era. *Genome Biol.* **15**, 523 (2014).
52. Kim, Y. H. et al. Combined microarray analysis of small cell lung cancer reveals altered apoptotic balance and distinct expression signatures of MYC family gene amplification. *Oncogene* **25**, 130–138 (2006).

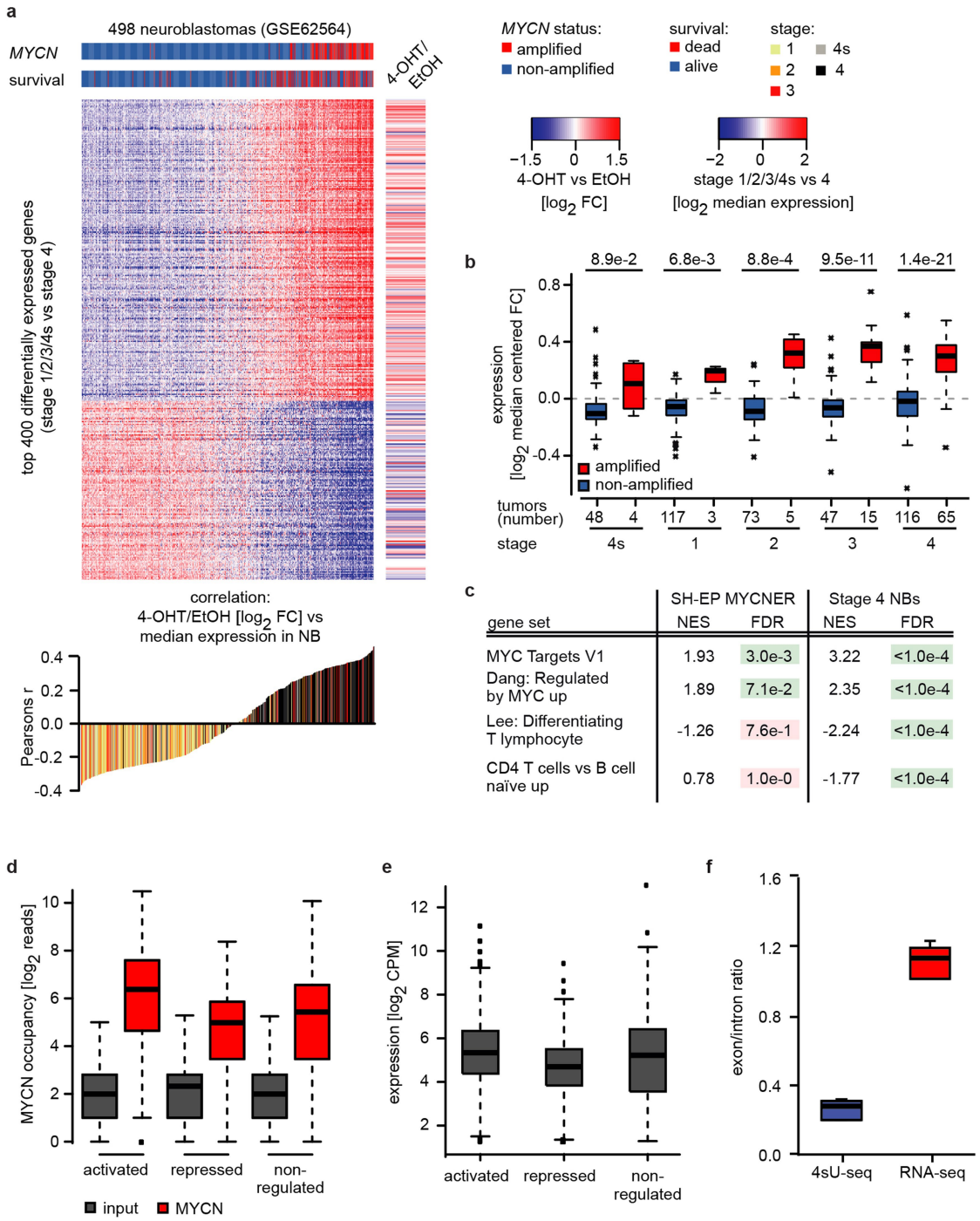

Extended Data Fig. 1 | Characterization of SH-EP MYCN–ER cells. **a**, Top, heat map showing the 400 most-differentially expressed genes between 498 low- and high-grade neuroblastomas (GSE62564). *MYCN* amplification status of the tumours and survival of the patients is indicated by the horizontal bars on top and the right panel illustrates gene expression changes after MYCN–ER activation (3 h 4-OHT), in SH-EP cells, of the same genes. Bottom, correlation between relative gene expression in tumours and changes in response to MYCN–ER activation. FC, fold change; NB, neuroblastoma. **b**, Box plots showing expression of 294 MYCN–ER-activated genes (SH-EP MYCN–ER, false-discovery rate (FDR) < 0.01 and $\log_2$((fold change in expression of 4-OHT compared to ethanol) > 0 in $n = 3$ biological replicates) in neuroblastomas of the indicated tumour stage with or without *MYCN* amplification (GSE62564). The number of tumour samples is indicated at the bottom and *P* values were calculated using a two-tailed Wilcoxon rank-sum test. **c**, Expression of selected gene sets from gene set enrichment analysis in SH-EP cells after MYCN–ER activation (3 h 4-OHT, $n = 3$) and in 65 *MYCN*-amplified versus 116 non-amplified stage 4 neuroblastomas (GSE62564). *P* values were calculated using a Kolmogorov–Smirnov test with 1,000 permutations and corrected for multiple testing using Benjamini–Hochberg procedure (FDR)[49]. NES, normalized enrichment score. **d**, Box plot illustrating MYCN binding to promoters (−30 to +300 bp relative to TSS) of 914 MYCN-activated and 615 repressed genes ($n = 3$). As control, a randomly selected group of 1,000 non-regulated expressed genes was chosen. **e**, Box plot illustrating mRNA levels in gene groups described above (activated, repressed and non-regulated; $n = 3$). **f**, Box plot showing the exon/intron ratio for 27,369 genes in 4sU-seq data ($n = 6$) compared to RNA-sequencing data ($n = 6$). **b**, **d**–**f**, In the box plots, the central line reflects the median and the borders of the boxes show the interquartile range of the plotted data. The whiskers extend to 1.5× the interquartile range and outliers are shown as dots.

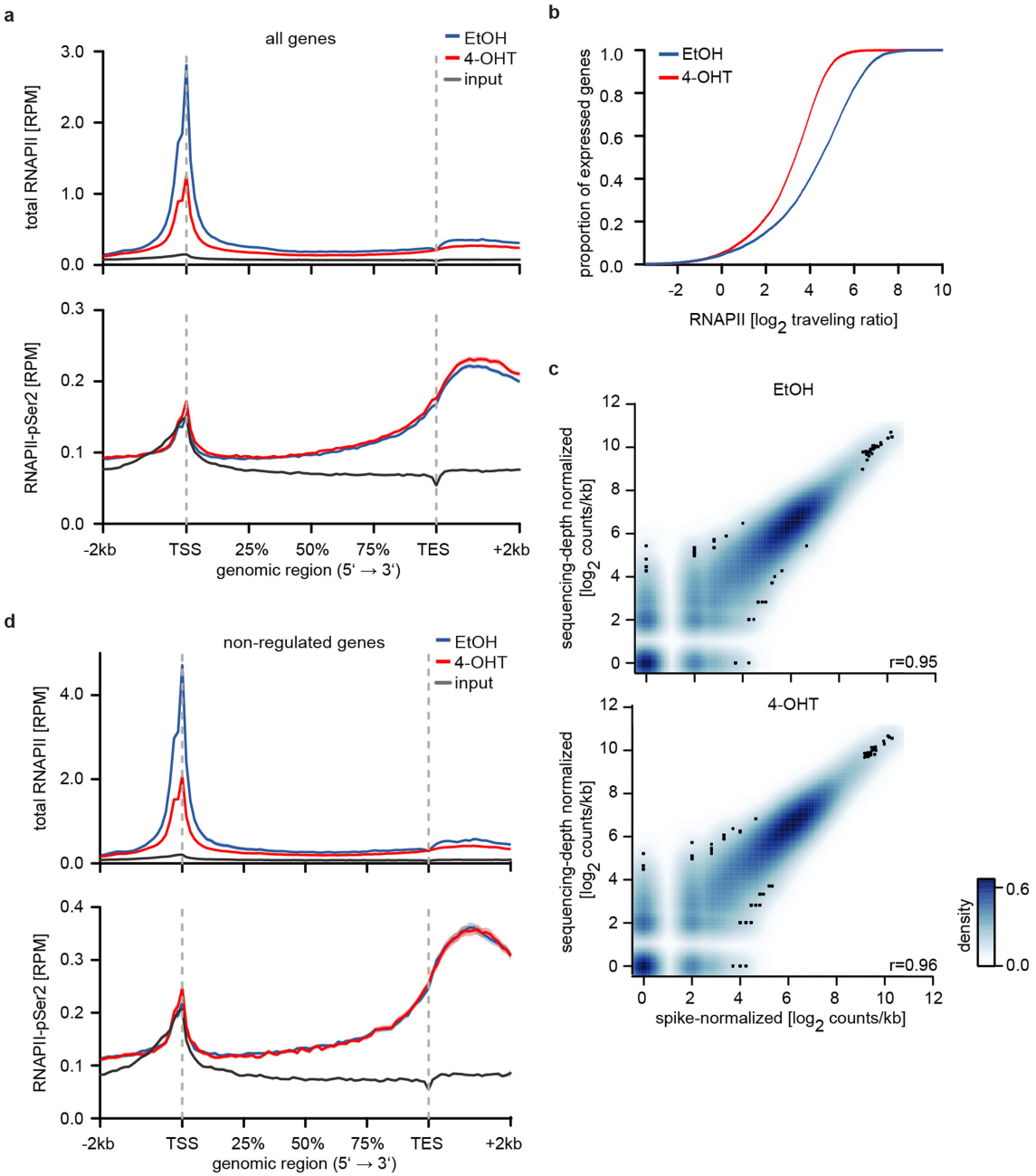

Extended Data Fig. 2 | Effects of MYCN on RNAPII function. **a**, Metagene plots of total RNAPII (top) and RNAPII(pSer2) (bottom) in SH-EP MYCN–ER cells after 4-OHT treatment (3 h) for 14,488 expressed genes ($n = 4$). Data are mean ± s.e.m. **b**, Empirical cumulative distribution function of RNAPII travelling ratio after MYCN–ER activation (4-OHT) of 14,488 expressed genes ($n = 4$). **c**, Two-dimensional kernel density plot of total RNAPII occupancy at the TSS of 14,945 expressed genes in SH-EP MYCN–ER cells treated with ethanol (top) or after activation of MYCN (bottom). Samples are normalized either to sequencing depth or using a mouse spike-in ($n = 1$). *r*, Pearson's correlation coefficient. **d**, Metagene plots of total RNAPII (top) and RNAPII(pSer2) (bottom) in SH-EP MYCN–ER cells after 4-OHT treatment (3 h; $n = 4$) of 1,000 non-regulated genes. Data are mean ± s.e.m.

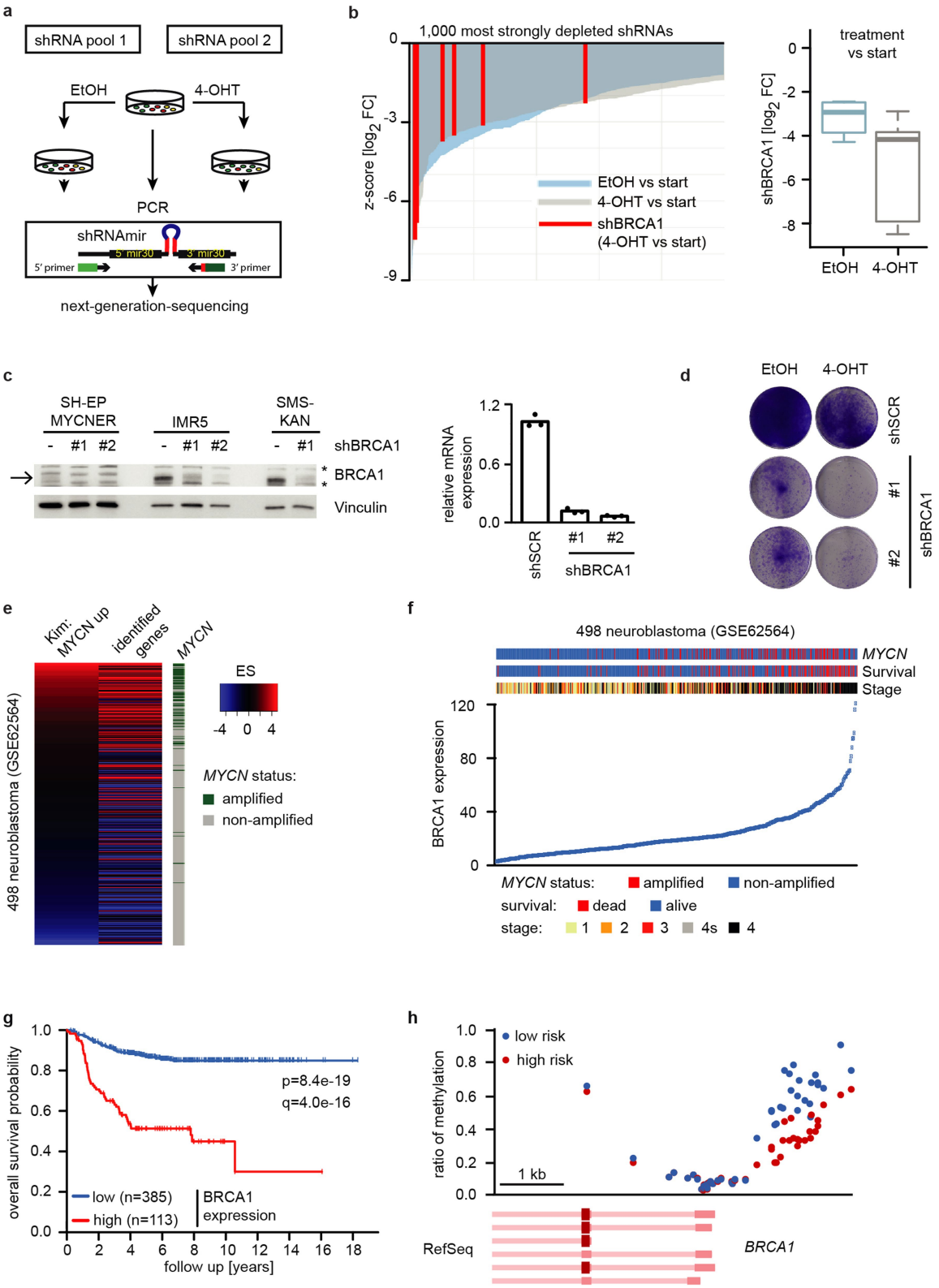

Extended Data Fig. 3 | See next page for caption.

Extended Data Fig. 3 | Characterization of BRCA1 function in neuroblastoma. a, Schematic overview of the shRNA screen in SH-EP MYCN–ER cells. Samples were analysed in duplicates after 14 days of cell culture. **b**, Waterfall plot (left) visualizing the depletion of the six screened shRNAs targeting *BRCA1* in SH-EP MYCN–ER cells with activated MYCN (*Z*-score for the $\log_2$(fold change in expression of 4-OHT compared to start)). From all 12,931 individual shRNA, only the 1,000 shRNAs that were most strongly depleted in the screen following 4-OHT treatment are shown. *Z*-scores for the depletion of all individual shRNAs were calculated on the basis of the population mean and s.d. of the $\log_2$(fold change in expression) of all screened shRNAs ($n = 2$). Box plot (right) comparing depletion of all shRNAs targeting *BRCA1* in SH-EP MYCN–ER cells upon activation of MYCN. The median and the lower and upper quartiles are shown, of the $\log_2$(fold change in expression of 4-OHT compared to start and ethanol compared to start) for $n = 6$ independent shRNAs targeting *BRCA1* mRNA. Whiskers extend to 1.5× interquartile range above and below the upper and lower quartiles, respectively. **c**, Immunoblot (left) of BRCA1 in SH-EP MYCN–ER and in *MYCN*-amplified IMR5 and SMS-KAN cells showing the knockdown of *BRCA1* by two shRNAs. Note the high BRCA1 levels in *MYCN*-amplified neuroblastoma cell lines (IMR5 and SMS-KAN) relative to the non-*MYCN*-amplified cell line (SH-EP). The arrow points to the BRCA1 band, asterisks denote unspecific bands. Vinculin was used as loading control. For all gel source data, see Supplementary Fig. 1. qPCR (right) of *BRCA1* mRNA levels in *BRCA1*-depleted SH-EP MYCN–ER cells. Data are mean of technical triplicates ($n = 3$). **d**, Clonogenic assay in SH-EP MYCN–ER cells after shRNA-mediated knockdown of *BRCA1* and induction of MYCN for six days. Colonies were stained with crystal violet ($n = 3$). **e**, Expression of a gene set of the 99 genes, identified in the shRNA screen, in patients with primary neuroblastoma. Each patient is ranked using a defined gene set of *MYCN*-amplified tumours[52]. *MYCN* amplification status of all 498 patients is indicated on the right. **f**, *BRCA1* gene expression in 498 neuroblastoma samples (GSE62564). Tumours are sorted on the basis of *BRCA1* expression. **g**, Survival of 498 patients with neuroblastoma (GSE62564) stratified by *BRCA1* expression. Data were obtained from GEO and the R2 platform was used for grouping tumour samples by scanning mode based on *BRCA1* expression. The *q* value reflects a Bonferroni-corrected *P* value (log-rank test). **h**, *BRCA1* genomic region around the TSS with average methylation status in high- versus low-risk neuroblastoma.

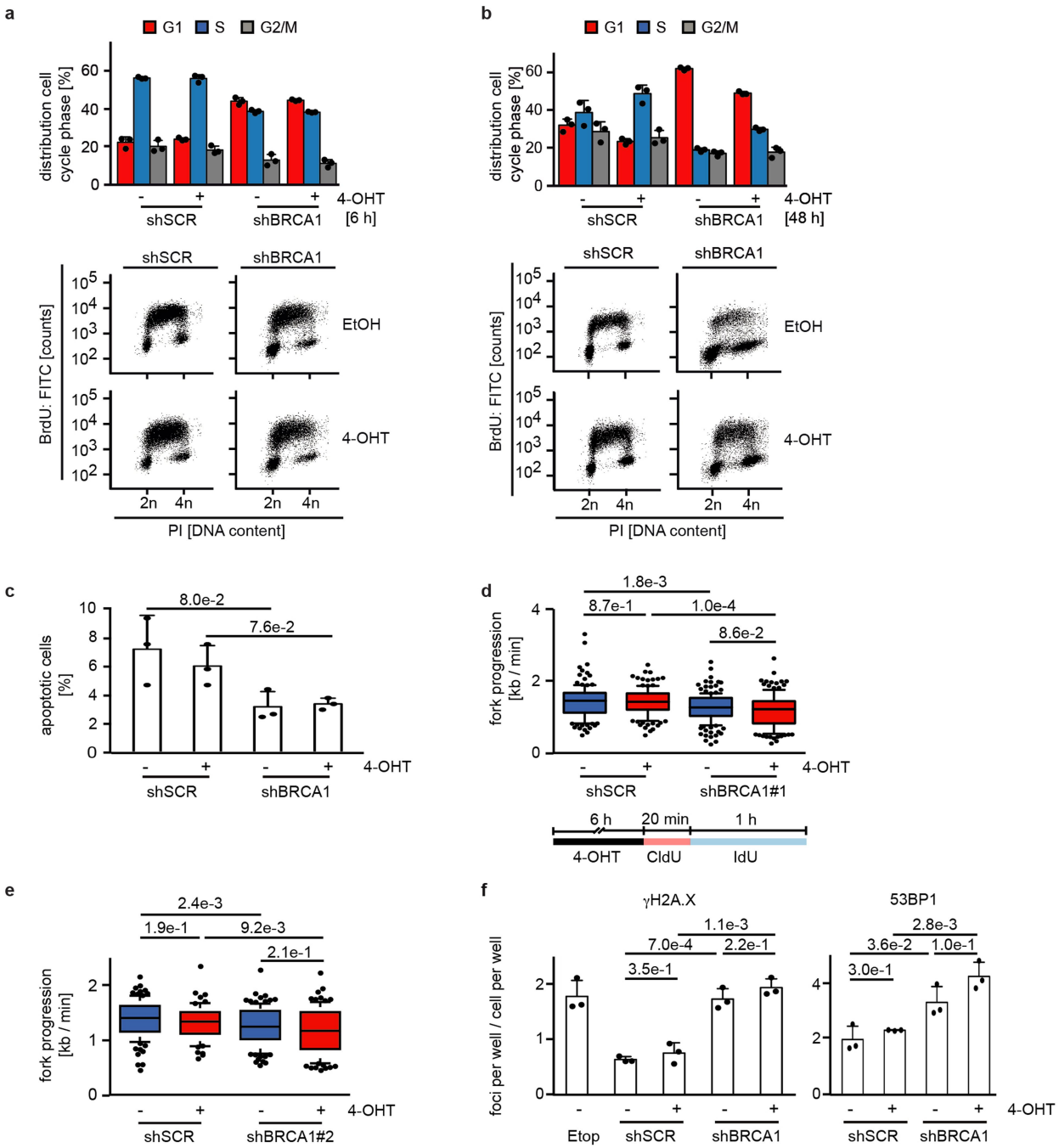

Extended Data Fig. 4 | Cell-cycle progression and DNA replication in SH-EP MYCN–ER cells. a, Quantification (top) and representative FACS profiles (bottom) documenting cell-cycle distribution of BrdU/propidium iodide (PI)-stained control and *BRCA1*-deficient cells treated with *BRCA1* shRNA 2 (shBRCA1#2) after 6 h of 4-OHT treatment. Propidium iodide staining was used for quantification. Data are mean + s.d. of biological triplicates. **b**, Same experimental set-up as in **a**, but after 48 h 4-OHT treatment. **c**, Percentage of apoptotic cells in control and *BRCA1*-deficient cells treated with shBRCA1#2 measured in a propidium iodide/annexin V FACS experiment after treatment with 4-OHT for 48 h. Data are mean + s.d. of biological triplicates. *P* values were calculated using an unpaired, two-tailed *t*-test. **d**, Top, fork progression rates during both labels based on the track length under the indicated conditions in control and *BRCA1*-deficient cells for *BRCA1* shRNA 1 (shBRCA1#1). The number of analysed DNA fibres is as follows: scramble shRNA (shSCR): ethanol, $n = 130$, 4-OHT $n = 131$; shBRCA1#1: ethanol, $n = 161$, 4-OHT, $n = 139$. *P* values were calculated using a two-tailed, unpaired *t*-test with additional Welch's correction. One representative experiment is shown ($n = 3$). Bottom, schematic of DNA fibre experiment labelled with CldU (red) and IdU (blue). **e**, Same experimental set-up as in **d** with shBRCA1#2. The number of DNA fibres is as follows: shSCR: ethanol, $n = 95$, 4-OHT, $n = 69$; shBRCA1#2: ethanol, $n = 109$, 4-OHT, $n = 90$. *P* values were calculated using a two-tailed, unpaired *t*-test with additional Welch's correction. One representative experiment is shown ($n = 3$). **d**, **e**, Fork progressions are displayed as box plots with the central line reflecting the median; the borders of the boxes show the lower and upper quartile of the plotted data, with 10th–90th-percentile whiskers and outliers are shown as dots. **f**, Number of γH2A.X (left) and 53BP1 (right) foci per well/number of cells per well, indicating DNA damage in control and *BRCA1*-deficient cells treated with shBRCA1#2 after 24 h of 4-OHT treatment. Etoposide (Etop; 25 μM) was used as a positive control and added for the final 2 h. Data are mean + s.d. of biological triplicates. *P* values were calculated using an unpaired, two-tailed *t*-test. One representative experiment is shown ($n = 3$).

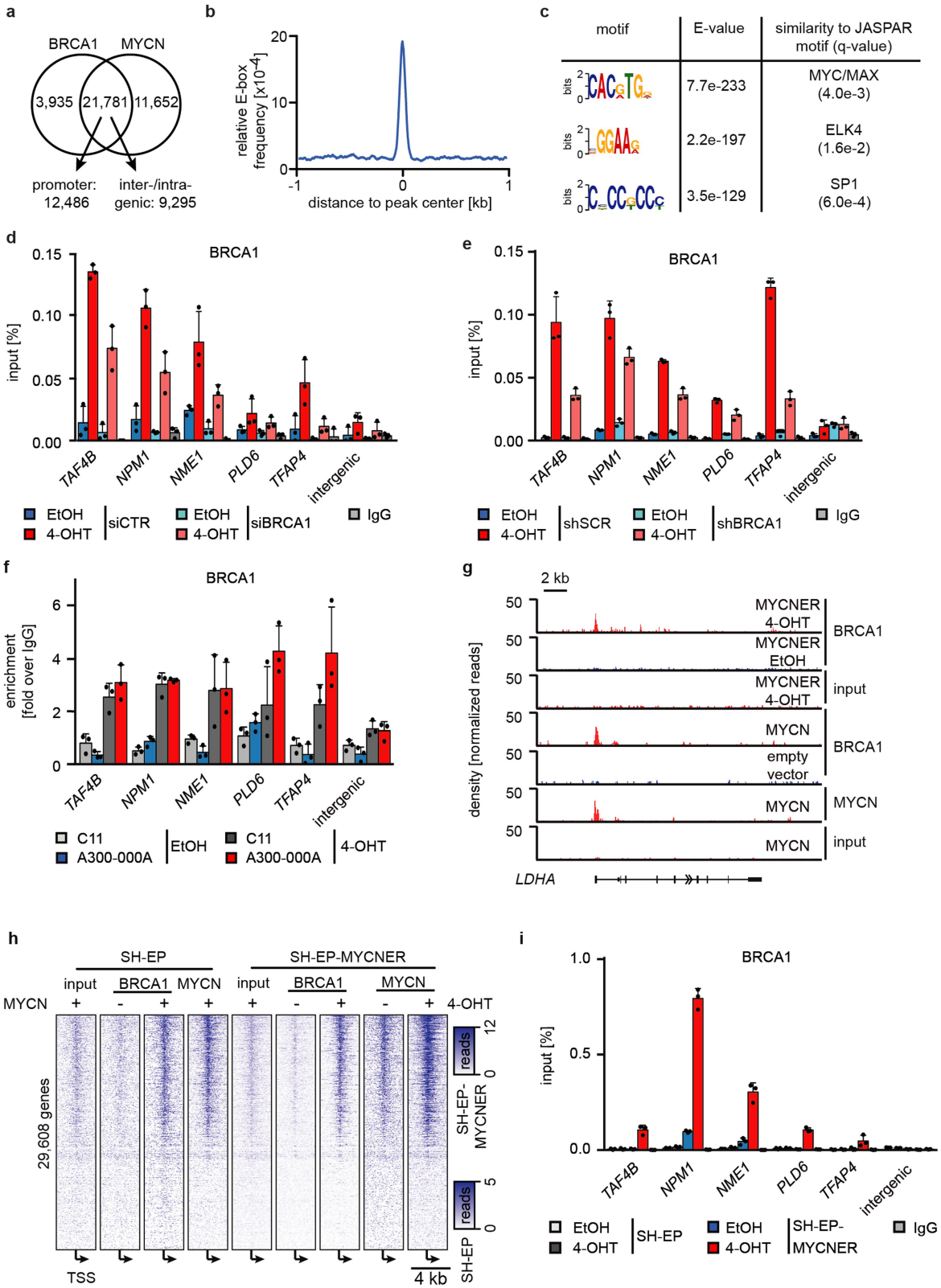

Extended Data Fig. 5 | See next page for caption.

Extended Data Fig. 5 | Control experiments for BRCA1 recruitment. **a**, Venn diagram documenting genome-wide overlap between BRCA1 and MYCN peaks. **b**, Relative E-box (CACGTG) frequency around BRCA1 peaks in promoter regions (±1 kb relative to the TSS). The curve is smoothed using a sliding window of 50 bp. **c**, Enriched DNA motifs in 12,161 BRCA1 peaks located in the promoter (±1 kb relative to the TSS) identified by de novo motif search. A region of ±50 bp around the BRCA1 peak summit was analysed and similarity to known motifs was assigned with TOMTOM and the JASPAR vertebrate motif database. *E* values are calculated with Fisher's exact test corrected for the number of input sequences, and *q* values for the comparison to known motifs are FDR-corrected *P* values calculated with a null model based on sampling motif columns from all of the columns in the set of target motifs[42]. The top three motifs from DREME analysis are shown ($n = 3$). **d**, ChIP of BRCA1 from SH-EP MYCN–ER cells transfected either with a control siRNA (siCTR) or siRNA targeting *BRCA1*. Selected promoters have both a robust MYCN and an overlapping BRCA1 peak. IgG was used as control. Where indicated, 4-OHT or ethanol was added for 5 h. Data are mean + s.d. of technical triplicates ($n = 1$). **e**, ChIP of BRCA1 from SH-EP MYCN–ER cells that stably express either a control shRNA or shRNA targeting *BRCA1*. IgG was used as control. The experiment was carried out as in **d**. Data are mean + s.d. of technical triplicates ($n = 1$). **f**, ChIP of BRCA1 from SH-EP MYCN–ER cells using two different BRCA1 antibodies. 4-OHT was added for 5 h. Data are mean + s.d. of the enrichment over IgG (of technical triplicates) ($n = 1$). **g**, Browser track of the *LDHA* locus of a BRCA1 and MYCN ChIP–seq experiment documenting BRCA1 binding to the *LDHA* promoter in SH-EP MYCN–ER cells after MYCN activation (5 h), and in SH-EP cells that express ectopic MYCN or empty vector as control. For ectopically expressing cells, the MYCN browser track is shown. **h**, Heat map showing occupancy of BRCA1 and MYCN in SH-EP MYCN–ER cells and SH-EP cells that express ectopic MYCN or empty vector as a control. Plot is centred to TSS. **i**, ChIP of BRCA1 from control SH-EP and from SH-EP MYCN–ER cells treated with either 4-OHT or ethanol (5 h). Data are mean + s.d. of technical triplicates of one representative experiment ($n = 2$).

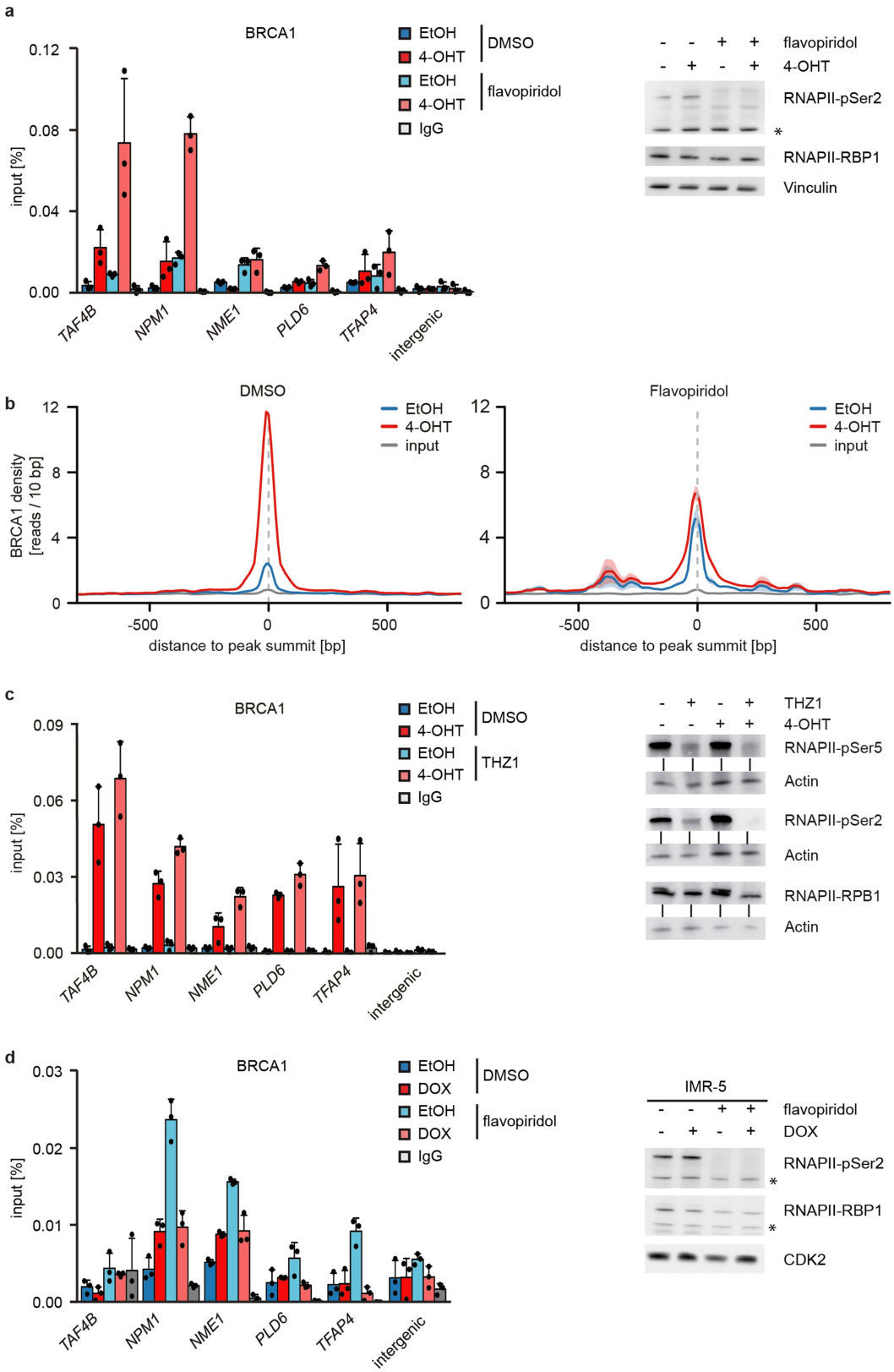

Extended Data Fig. 6 | See next page for caption.

Extended Data Fig. 6 | BRCA1 recruitment to paused RNAPII. a, Left, ChIP of BRCA1 at the indicated loci upon treatment of SH-EP MYCN–ER cells with 4-OHT (5 h) and flavopiridol (100 nM, 3 h), where indicated. Data are mean + s.d. of technical triplicates of one representative experiment ($n = 2$). Right, immunoblot of cells treated as described. Asterisk denotes an unspecific band. Vinculin was used as loading control ($n = 1$). **b**, Density plots of BRCA1 occupancy in 6,887 intergenic regions after treatment with either 4-OHT or ethanol (5 h) in DMSO-treated cells (left) and flavopiridol-treated cells (100 nM, 3 h) (right). Data are mean ± s.e.m. ($n = 1$). **c**, Left, ChIP of BRCA1 in SH-EP MYCN–ER cells treated with CDK7 inhibitor THZ1 (200 nM, 4 h) or DMSO as control together with 4-OHT or ethanol. Data are mean + s.d. of technical triplicates. Right, immunoblots for RNAPII(pSer5), RNAPII(pSer2) and total RNAPII after treatment as described above. Actin was used as loading control ($n = 1$). **d**, Left, ChIP of BRCA1 at the indicated loci in *MYCN*-amplified IMR-5 neuroblastoma cells that express a doxycycline (DOX)-inducible shRNA targeting *MYCN*. Where indicated, cells were treated with flavopiridol (200 nM, 4 h) or doxycycline (1 $\mu g\ ml^{-1}$, 48 h). Data are mean + s.d. of technical triplicates of one representative experiment ($n = 2$). Right, immunoblot of cells treated as described above. Asterisks denote unspecific bands. CDK2 was used as loading control ($n = 2$).

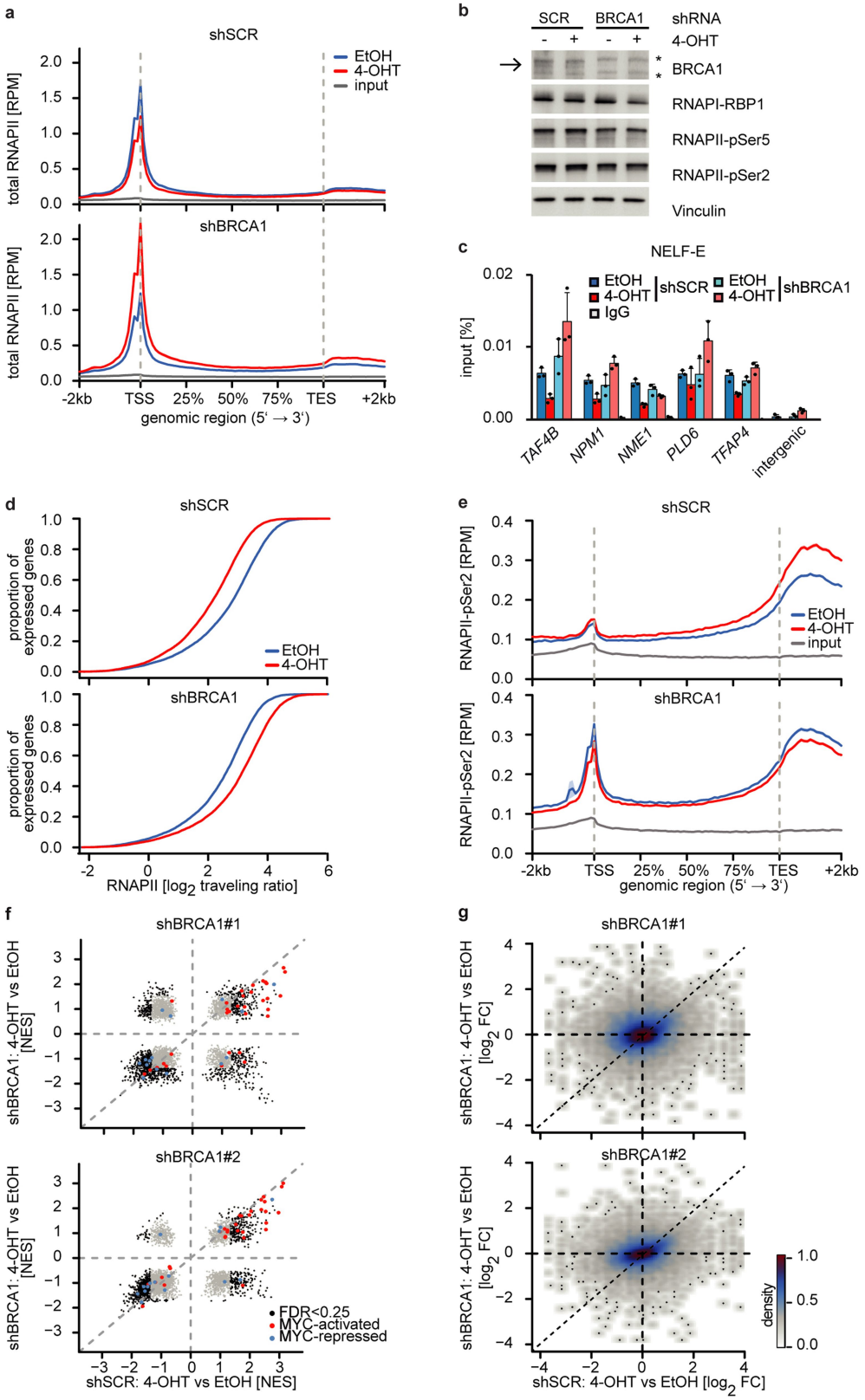

Extended Data Fig. 7 | See next page for caption.

Extended Data Fig. 7 | Effect of BRCA1 on MYCN-dependent RNAPII function. a, Metagene plots of total RNAPII after 4-OHT treatment (3 h) in control (top) and *BRCA1*-depleted cells treated with shBRCA1#1 (bottom) on 14,488 expressed genes. Data are mean ± s.e.m. **b**, Immunoblot of total RNAPII (RBP1) and phosphorylated forms after knockdown of *BRCA1* and activation of MYCN. One representative experiment is shown ($n = 2$). The arrow points to the BRCA1 band, asterisks denote unspecific bands. **c**, ChIP of NELF-E in control and *BRCA1*-depleted SH-EP MYCN–ER cells after 4-OHT treatment (4 h). Data are mean + s.d. of technical triplicates of one representative experiment ($n = 3$ using two different shRNAs). **d**, Empirical cumulative distribution function of RNAPII travelling ratio after MYCN–ER activation (3 h) in control (top) and *BRCA1*-depleted (bottom) cells treated with shBRCA1#2 of 14,488 expressed genes. **e**, Metagene plots (of RNAPII(pSer2) in control (top) and *BRCA1*-depleted (bottom) cells treated with shBRCA1#2 upon treatment as described above for 14,488 expressed genes. Data are mean ± s.e.m. **f**, Gene set enrichment analysis upon activation of MYCN (5 h) in *BRCA1*-depleted and control conditions ($n = 3$). Significantly enriched gene sets are highlighted in black (FDR $q < 0.25$), MYC-activated gene sets are marked in red and MYC-repressed gene sets are marked in blue. FDR was calculated using a Kolmogorov–Smirnov test with 1,000 permutations using a Benjamini–Hochberg correction for multiple testing. **g**, Two-dimensional kernel density plot correlating gene expression changes after MYCN–ER activation (5 h) in *BRCA1*-depleted and control cells. Results are shown for two shRNAs of 19,429 expressed genes. *r*, Pearson's correlation coefficient.

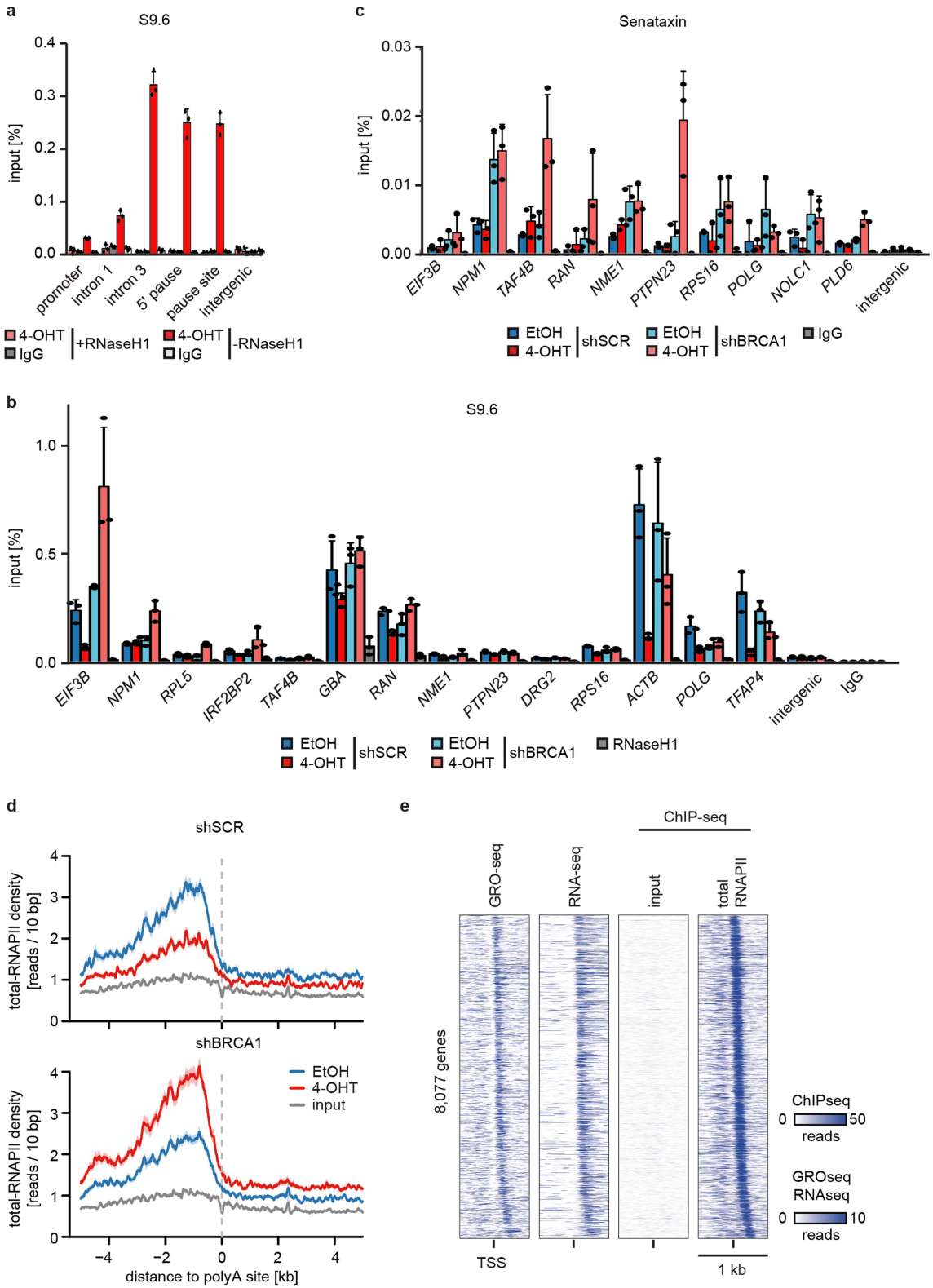

Extended Data Fig. 8 | BRCA1 promotes R-loop resolution and mRNA decapping. a, DRIP using the S9.6 antibody, indicating R-loops at known loci within the *ACTB* gene. Digestion with RNase H1 was used as control for specificity of the antibody and IgG as control for unspecific chromatin binding. Data are mean + s.d. of technical triplicates of one representative experiment ($n = 2$). **b**, DRIP documenting binding of the S9.6 R-loop antibody to the indicated loci upon depletion of *BRCA1* and activation of MYCN for 4 h. Data are mean + s.d. of technical triplicates of one representative experiment ($n = 4$). The panel shows the non-normalized data of Fig. 3d. **c**, ChIP of senataxin at the indicated loci in SH-EP MYCN–ER cells after 4-OHT treatment (3 h) in control or *BRCA1*-depleted cells. Data are mean + s.d. of technical triplicates of one representative experiment ($n = 2$ with 2 different antibodies). **d**, RNAPII density around the first downstream polyA site in SH-EP MYCN–ER cells after *BRCA1* depletion using shBRCA1#2 and MYCN activation for 3 h: 1,713 genes are shown. Data are mean ± s.e.m. One representative experiment is shown ($n = 3$). **e**, Heat map of 8,077 TSSs of genes with an RNAPII peak downstream of the start site. Reads originate from GRO–seq, mRNA sequencing and total RNAPII ChIP–seq samples and genes are sorted on the basis of the distance from the TSS to the RNAPII peak.

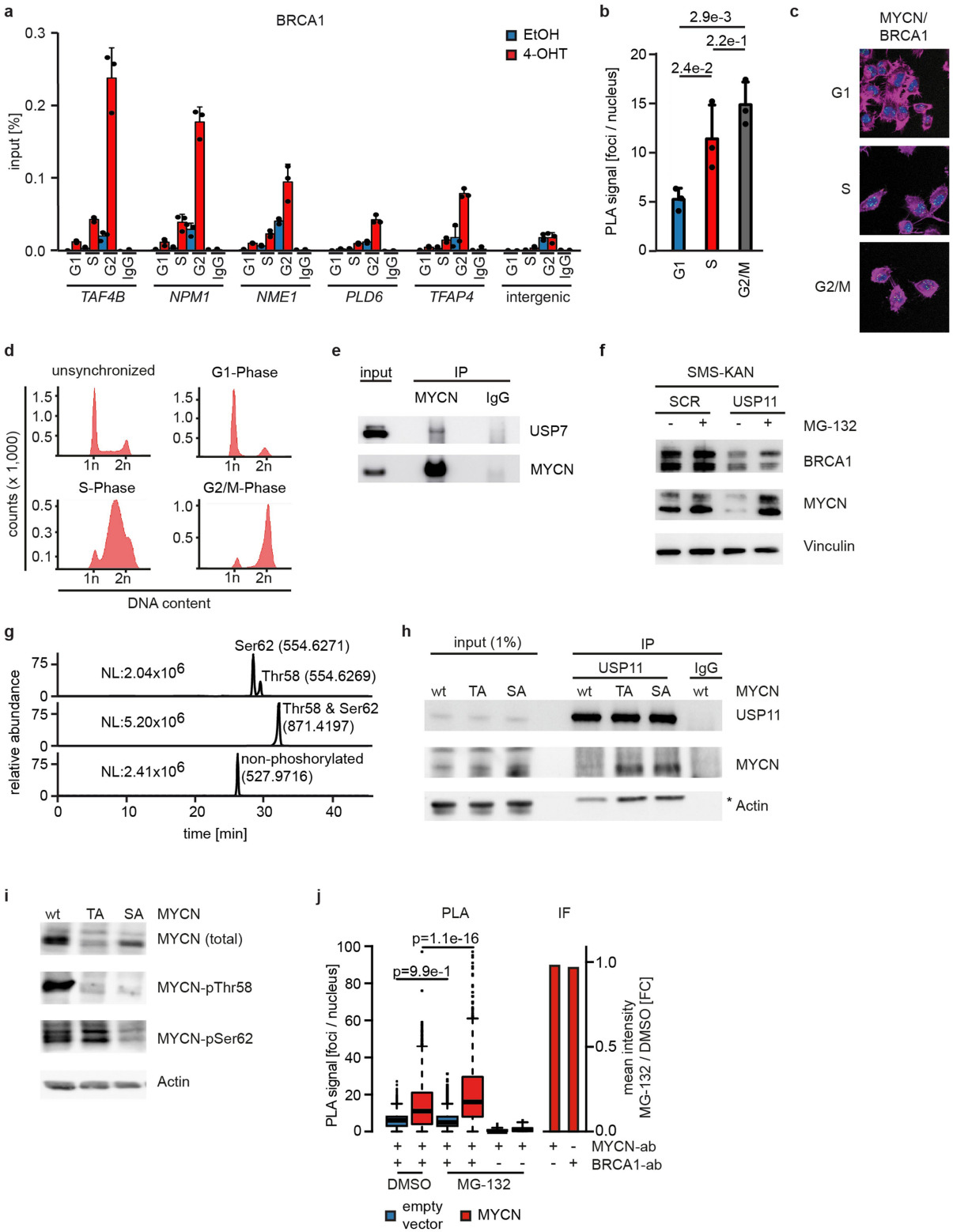

Extended Data Fig. 9 | See next page for caption.

Extended Data Fig. 9 | Characterization of BRCA1 recruitment and of the interaction of USP11 with MYCN. a, ChIP of BRCA1 in SH-EP MYCN–ER cells synchronized by a double thymidine block. Cells were released and collected during the indicated cell-cycle phase after 4 h of 4-OHT treatment. IgG was used as control. Data are mean + s.d. of technical triplicates ($n = 1$). **b**, Bar plot summarizing the PLAs of MYCN and BRCA1 in G1, S and G2 phases in SH-EP MYCN–ER cells synchronized as described in **a** and upon 3 h 4-OHT treatment. Data are mean + s.d. of biological triplicates. For each cell-cycle phase, between 74 and 276 cells were counted. *P* values were calculated using an unpaired, two-tailed *t*-test ($n = 1$). **c**, Representative pictures of the PLA from **b** showing proximity of MYCN and BRCA1 in G1, S and G2 phases (green dots). Nuclei were stained with Hoechst, cytoskeleton was stained using phalloidin indicated in violet ($n = 1$). **d**, Representative FACS profiles of propidium-iodide-stained SH-EP MYCN–ER cells used for the experiment in **a** ($n = 1$). **e**, Immunoblot of anti-MYCN immunoprecipitates from IMR-5 *MYCN*-amplified neuroblastoma cells. The input corresponds to 0.75% of the amount used for the precipitation. One representative experiment is shown ($n = 2$). **f**, Immunoblot of indicated proteins after knockdown of *USP11* in SMS-KAN cells and treatment with MG-132 (10 μM, 6 h), where indicated. Vinculin was used as loading control ($n = 1$). **g**, Extracted ion chromatogram of MYCN phosphorylation status from SH-EP cells that express ectopic MYCN. Values in parentheses indicate *m*/*z* ratio for each peak and the normalized target level (NL) is given for each chromatogram ($n = 1$). **h**, Immunoblot of anti-USP11 immunoprecipitates from SH-EP cells that stably express wild-type MYCN (wt), Thr58Ala (TA) or Ser62Ala (SA) mutants of MYCN. Asterisk denotes an unspecific band. One representative experiment is shown ($n = 3$). **i**, Immunoblot documenting phosphorylation status of the indicated alleles of MYCN. Actin was used as loading control. One representative experiment is shown ($n = 2$). **j**, Left, quantification of a PLA that illustrates complex formation of BRCA1 with MYCN in SH-EP cells that express ectopic MYCN or empty vector as control. Between 749 and 1,854 cells were counted for each condition. *P* values were calculated with a two-tailed Wilcoxon rank-sum test. In the box plot, the central line reflects the median and the borders of the boxes show the interquartile range of the plotted data. The whiskers extend to 1.5× the interquartile range, and outliers are shown as dots. Right, quantification of the corresponding immunofluorescence (IF) signals of the indicated antibodies ($n = 1$).

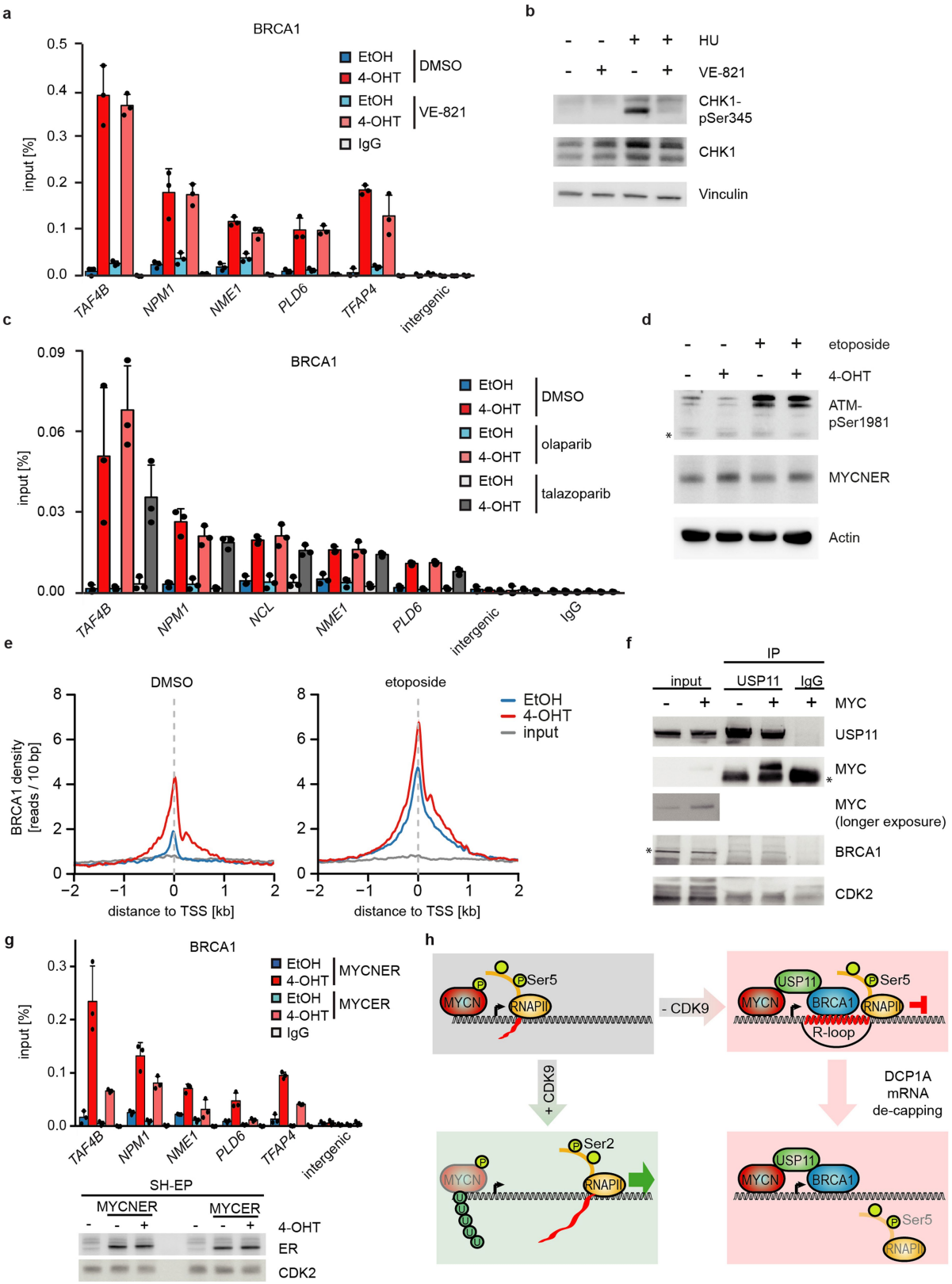

Extended Data Fig. 10 | See next page for caption.

Extended Data Fig. 10 | Role of DNA damage and of MYC in recruitment of BRCA1. a, ChIP of BRCA1 in SH-EP MYCN–ER cells that were pre-treated with ATR inhibitor VE-821 (1 μM, 2 h), 4-OHT or ethanol was added for 4 h. Data are mean + s.d. of technical triplicates of one representative experiment ($n = 2$). **b**, Immunoblot of CHK1(pSer345) after treatment with ATR inhibitor VE-821, as described in **a**. Cells were treated with HU (5 mM) for 4 h as positive control. Asterisk denotes an unspecific band. Vinculin was used as loading control. One representative experiment is shown ($n = 2$). **c**, ChIP of BRCA1 in SH-EP MYCN–ER cells at the indicated loci after treatment (9 h) with olaparib (10 μM), talazoparib (1 μM) or DMSO as control. Data are mean + s.d. of technical triplicates of one representative experiment ($n = 3$). **d**, Immunoblot of ATM(pSer1981) after treatment with etoposide (5 μM, 3 h). Actin was used as loading control ($n = 1$). **e**, Density plots of BRCA1 occupancy after treatment with either 4-OHT or ethanol (5 h) in DMSO (left) and etoposide-treated (right) SH-EP MYCN–ER cells. **f**, Immunoblots of anti-USP11 immunoprecipitates from either control SH-EP cells or cells transiently transfected with MYC. CDK2 was used as loading control, asterisks denote unspecific bands. The input corresponds to 2% of the amount used for the precipitation. One representative experiment is shown ($n = 3$). **g**, Left, ChIP of BRCA1 at the indicated loci in SH-EP MYCN–ER or SH-EP MYC–ER cells treated with 4-OHT (5 h) or ethanol. Data are mean + s.d. of technical triplicates of one representative experiment ($n = 2$). Right, immunoblot performed with the ER antibody to detect MYCN–ER and MYC–ER in SH-EP, SH-EP MYCN–ER or SH-EP MYC–ER cells treated with 4-OHT or ethanol. CDK2 was used as loading control ($n = 2$). **h**, Model illustrating our findings. We propose that BRCA1 is recruited jointly by MYCN and Ser5-phosphorylated RNAPII. BRCA1 recruitment is strongly enhanced by blockade of CDK9, which blocks pause release, and by increasing torsional stress using etoposide, which suggests that it is predominantly a stress response to stalling of RNAPII. BRCA1, in turn, is required to prevent an MYCN-dependent accumulation of stalling RNAPII and R-loop formation via a mRNA-decapping complex. The critical signal in MYCN that enables recruitment of BRCA1 is the dephosphorylation of Thr58, a residue that—when phosphorylated—is recognized by FBXW7 and promotes turnover of MYCN. Dephosphorylation of Thr58 allows binding of USP11, which stabilizes MYCN and BRCA1 on chromatin, which suggests that a kinetic competition between MYCN turnover and dephosphorylation/deubiquitination controls the fate of RNAPII at promoters.

nature research

Corresponding author(s): Steffi Herold, Martin Eilers

Reporting Summary

Nature Research wishes to improve the reproducibility of the work that we publish. This form provides structure for consistency and transparency in reporting. For further information on Nature Research policies, see Authors & Referees and the Editorial Policy Checklist.

Statistical parameters

When statistical analyses are reported, confirm that the following items are present in the relevant location (e.g. figure legend, table legend, main text, or Methods section).

n/a	Confirmed
☐	☒ The exact sample size (*n*) for each experimental group/condition, given as a discrete number and unit of measurement
☐	☒ An indication of whether measurements were taken from distinct samples or whether the same sample was measured repeatedly
☐	☒ The statistical test(s) used AND whether they are one- or two-sided *Only common tests should be described solely by name; describe more complex techniques in the Methods section.*
☐	☒ A description of all covariates tested
☐	☒ A description of any assumptions or corrections, such as tests of normality and adjustment for multiple comparisons
☐	☒ A full description of the statistics including central tendency (e.g. means) or other basic estimates (e.g. regression coefficient) AND variation (e.g. standard deviation) or associated estimates of uncertainty (e.g. confidence intervals)
☐	☒ For null hypothesis testing, the test statistic (e.g. *F*, *t*, *r*) with confidence intervals, effect sizes, degrees of freedom and *P* value noted *Give P values as exact values whenever suitable.*
☒	☐ For Bayesian analysis, information on the choice of priors and Markov chain Monte Carlo settings
☒	☐ For hierarchical and complex designs, identification of the appropriate level for tests and full reporting of outcomes
☒	☐ Estimates of effect sizes (e.g. Cohen's *d*, Pearson's *r*), indicating how they were calculated
☐	☒ Clearly defined error bars *State explicitly what error bars represent (e.g. SD, SE, CI)*

Our web collection on statistics for biologists may be useful.

Software and code

Policy information about availability of computer code

Data collection	Software was used for collection and analysis and is listed below.
Data analysis	FASTQ Generation software v1.0.0 http://illumina.com FastQC v0.11.3 http://www.bioinformatics.babraham.ac.uk/projects/fastqc/ Tophat v2.1.0 Kim D, Pertea G, Trapnell C, Pimentel H, Kelley R, Salzberg SL. TopHat2: accurate alignment of transcriptomes in the presence of insertions, deletions and gene fusions. Genome Biology 2013, 14:R36 Bowtie v1.2 Langmead B, Trapnell C, Pop M, Salzberg SL. Ultrafast and memory-efficient alignment of short DNA sequences to the human genome. Genome Biol 10:R25. Bowtie v2.3.2 Langmead B, Salzberg S. Fast gapped-read alignment with Bowtie 2. Nature Methods. 2012, 9:357-359. MACS v1.4.1 Zhang et al. Model-based Analysis of ChIP-Seq (MACS). Genome Biol (2008) vol. 9 (9) pp. R137 BEDtools v2.26.0 Quinlan AR, Hall IM. BEDTools: a flexible suite of utilities for comparing genomic features. Bioinformatics. 2010;26(6):841-842. SAMtools v1.3 Li H., Handsaker B., Wysoker A., Fennell T., Ruan J., Homer N., Marth G., Abecasis G., Durbin R. and 1000 Genome Project Data Processing Subgroup (2009) The Sequence alignment/map (SAM) format and SAMtools. Bioinformatics, 25, 2078-9. [PMID: 19505943] DeepTools v2.3.5 Ramírez F, Dündar F, Diehl S, Grüning BA, Manke T. deepTools: a flexible platform for exploring deep-sequencing data. Nucleic Acids Res. 2014 Jul;42:W187-91. NGSplot v2.61 Shen, L., Shao, N., Liu, X. and Nestler, E. (2014) ngs.plot: Quick mining and visualization of next-generation sequencing data by integrating genomic databases, BMC Genomics, 15, 284.

Integrated Genome Browser v9.0.0 Freese NH, Norris DC, Loraine AE. Integrated genome browser: visual analytics platform for genomics. Bioinformatics. Epub: 2016, March 16; 1-7. 10.1093/bioinformatics/btw069
MEME Suite v4.10.1 Timothy L. Bailey, Mikael Bodén, Fabian A. Buske, Martin Frith, Charles E. Grant, Luca Clementi, Jingyuan Ren, Wilfred W. Li, William S. Noble, "MEME SUITE: tools for motif discovery and searching", Nucleic Acids Research, 37:W202-W208, 2009.
R v3.3.3 R Core Team (2017). R: A language and environment for statistical computing. R Foundation for Statistical Computing, Vienna, Austria. URL https://www.R-project.org/.
EdgeR Robinson, MD, McCarthy, DJ, Smyth, GK (2010). edgeR: a Bioconductor package for differential expression analysis of digital gene expression data. Bioinformatics 26, 139–140.
GenomicAlignments Lawrence M, Huber W, Pages H, Aboyoun P, Carlson M, et al. (2013) Software for Computing and Annotating Genomic Ranges. PLoS Comput Biol 9(8): e1003118. doi:10.1371/journal.pcbi.1003118
GSEA v2.2.0 Aravind Subramanian, Pablo Tamayo, Vamsi K. Mootha, Sayan Mukherjee, Benjamin L. Ebert, Michael A. Gillette, Amanda Paulovich, Scott L. Pomeroy, Todd R. Golub, Eric S. Lander, and Jill P. Mesirova. Gene set enrichment analysis: A knowledge-based approach for interpreting genome-wide expression profiles. PNAS 2005 vol. 102 no. 43, 15545–15550, doi: 10.1073/pnas.0506580102
MSigDB v5.2 Arthur Liberzon, Aravind Subramanian, Reid Pinchback, Helga Thorvaldsdóttir, Pablo Tamayo, Jill P. Mesirov. Molecular signatures database (MSigDB) 3.0. Bioinformatics, 2011 June 15; 1739–1740
skewR Ginno, P. A., Lott, P. L., Christensen, H. C., Korf, I. & Chedin, F. R-loop formation is a distinctive characteristic of unmethylated human CpG island promoters. Mol Cell 45, 814-825, doi:10.1016/j.molcel.2012.01.017 (2012).
CASAVA v1.7 http://emea.support.illumina.com/downloads/casava_software_version_18_user_guide_(15011196_b).html?langsel=/de/
ImageJ v1.50j http://imagej.nih.gov/ij
GraphPad Prism v5, v6 for Mac https://www.graphpad.com/scientific-software/prism/
ZEN 2 (blue edition), https://www.zeiss.com/microscopy/int/products/microscope-software/zen-2-core.html
Harmony High Content Imaging and Analysis Software, http://www.perkinelmer.de/product/harmony-4-8-office-hh17000001
StepOne software v2.3, https://www.thermofisher.com/de/de/home/technical-resources/software-downloads/StepOne-and-StepOnePlus-Real-Time-PCR-System.html
Multi Gauge software v3.0 https://cloudfront.ualberta.ca/-/media/science/departments/biological-sciences/mbsu/fla-5000/mulitgauge20.pdf
BD FACSDIVA Software v6.1.2 http://www.bdbiosciences.com/us/instruments/research/software/flow-cytometry-acquisition/bd-facsdiva-software/m/111112/overview

For manuscripts utilizing custom algorithms or software that are central to the research but not yet described in published literature, software must be made available to editors/reviewers upon request. We strongly encourage code deposition in a community repository (e.g. GitHub). See the Nature Research guidelines for submitting code & software for further information.

Data

Policy information about availability of data

All manuscripts must include a data availability statement. This statement should provide the following information, where applicable:

- Accession codes, unique identifiers, or web links for publicly available datasets
- A list of figures that have associated raw data
- A description of any restrictions on data availability

ChIP- and mRNA-sequencing datasets as well as results from the shRNA screen are available at the Gene Expression Omnibus under the accession number GEO: GSE111905.
4sU-sequencing data is available at the Gene Expression Omnibus under the accession number GEO: GSE113861.

Field-specific reporting

Please select the best fit for your research. If you are not sure, read the appropriate sections before making your selection.

☒ Life sciences ☐ Behavioural & social sciences

For a reference copy of the document with all sections, see nature.com/authors/policies/ReportingSummary-flat.pdf

Life sciences

Study design

All studies must disclose on these points even when the disclosure is negative.

Sample size	For RNA-seq experiments, sample size was not determined since an a priori power analysis involves knowledge about the expected effect size which is impossible to estimate beforehand. From multiple experiments we know that triplicates are sufficient to give statistical significant results which are accorded in literature (Walz, S. et al.; Jaenicke, L. A. et al.) For all other experiments, sample size calculation was not applicable.
Data exclusions	No data was excluded from the analysis.
Replication	Most experiments were done in biological duplicates or triplicates with reproducible results. We did not exclude any replicates. Ch-IP Seq experiments for BRCA1 recruitment in flavopiridol- or etoposide treated cells and SH-EP cells expressing ectopic MYCN as well as Ch-IP Seq experiment for MYCN recruitment in BRCA1 knockdown cells are single experiments. For each experiment we state the number of independent replications in the figure legend.

Randomization	Randomization was not applicable for our study since we do not report experiments involving animals or patients.
Blinding	Blinding was not applicable for our study since we do not report relevant experiments.

Materials & experimental systems

Policy information about availability of materials

n/a	Involved in the study
☒	☐ Unique materials
☐	☒ Antibodies
☐	☒ Eukaryotic cell lines
☒	☐ Research animals
☒	☐ Human research participants

Antibodies

Antibodies used

primary antibodies:
MYCN; Santa Cruz Cat #sc-791; C-19; Lot: A0915
MYCN; Santa Cruz Cat #sc-53993; B8.4.B; Lot: C1218
MYCN; Santa Cruz Cat #sc-56729; NCM II 100; Lot: F0413
BRCA1; Bethyl Laboratories Cat #A300-000A; Lot: 000A-2
BRCA1; Santa Cruz Cat #sc-514797; C-11
BRCA1; Sigma-Aldrich Cat #07-434; Charge: 20189179
CDK2; Santa Cruz Cat #sc-6248; D-12; Lot: B0916
ER; Santa Cruz Cat #sc-8002; F-10; Lot: K-2316
RNAPII (RPB1); Santa Cruz Cat #sc-899; N-20; Lot: C1815:
RNAPII (RPB1); Santa Cruz Cat #sc-17798; A-10; Lot: B1516 / B0717
RNAPII (RPB1); Covance # MMS-126R-500; Ch-Nr.: B200433
p-RNAPII (Ser2); abcam Cat #ab5095; Lot: GR3172948-1
p-RNAPII (Ser5); Covance Cat #MMS-128P; Chage: B208777
Anti DNA-RNA Hybrid; Stephen H. Leppla, NIH; S9.6
Anti DNA-RNA Hybrid; Kerafast Cat #ENH001; S9.6; Lot: 071718_1
USP11; Bethyl Laboratories Cat #A301-613A; Lot: 613A-1
Beta-Actin; Sigma-Aldrich Cat #A5441; AC-15; Lot: 014M4759
Vinculin; Sigma-Aldrich Cat #V9131; hVIN-1; Lot # F0413
p-H2A.X (Ser139); Cell Signaling Cat #2577; Lot: 1922552
53BP1; Santa Cruz Cat #sc-22760; H-300
USP7; Bethyl Laboratories Cat #A300-033A; Lot: A300-033A-8
c-MYC; abcam Cat #ab32072; Y69; Lot: GR3232703-5/-6/-9/-10
DCP1A; Santa Cruz Cat #sc-100706; 56-Y; Lot: G3018
CHK1; Santa Cruz Cat #sc-7898; FL-476; Lot: 0412
p-CHK1 (Ser345); Cell Signaling Cat #2348; Lot: 18
p-ATM (Ser1981); Merck Cat #MAB3806; 10H11.E12
Tubulin; Merck Cat #MAB1637; TU-20
BrdU; AbD Serotec, Cat #MCA2060; Clone BU1/75
BrdU; abcam Cat #ab6326; Clone BU1/75
BrdU; BD Biosciences Cat #: 347580; Clone B44
BrdU; Santa Cruz Cat #sc-32323; Clone IIB5; Lot: J0417
FITC anti-BrdU; Biozol/BioLegend Cat #BLD-364104; Clone: 3D4
NELF-E; Merck Cat #ABE48; Lot: 2762234
Senataxin; Novus Biologicals Cat #NB100-57542; Lot: A3
Senataxin; Bethyl Laboratories Cat #A301-104A; Lot: 104A-2

secondary antibodies:
Immunoblots: ECLTM Anti Rb IgG HRP linked GE Healthcare Cat #NA934(V)
ECLTM Anti Ms IgG HRP linked GE Healthcare Cat #NA931(V)
Immunofluorescence: Alexa Fluor 647 Goat anti-Rabbit IgG (H+L); Invitrogen Cat #A-21244
DNA fiber assay: Alexa Fluor 555, Goat anti-Rat IgG (H+L); Invitrogen Cat #A-21434
Alexa Fluor 488, Goat anti-Mouse IgG (H+L); Invitrogen Cat # A-11029

Dilutions:
IB: primary antibody: 1:1,000
secondary antibody: 1:3,000

FACS: FITC anti-BrdU: 5µl/10^6 cells

PLA: RNAPII (RBP1, Covance) 1:1,000; p-RNAPII (Ser2) 1:500; p-RNAPII (Ser5) 1:1,000;
BRCA1 (Bethyl Laboratories) 1:500; BRCA1 (Santa Cruz) 1:500; MYCN; Santa Cruz Cat #sc-56729 1:300

Immunofluorescence: primary antibody: p-H2A.X (Ser139) 1: 400; 53BP1 1:500

secondary antibody: 1:400

DNA fiber assay: primary antibody: BrdU (AbD Serotec) 1:400; BrdU (abcam) 1:400; BrdU (BD Biosciences) 1:150
secondary antibody: 1:150

Validation

Antibodies for Immunoblots:
MYCN; Santa Cruz Cat #sc-791 validated by shRNA
BRCA1; Sigma-Aldrich Cat #07-434 validated by shRNA
p-RNAPII (Ser2); abcam Cat #ab5095 validated by THZ treatment and flavopiridol treatment
p-RNAPII (Ser5); Covance Cat #MMS-128P validated by THZ treatment
USP11; Bethyl Laboratories Cat #A301-613A validated by shRNA

Antibodies for Immunoprecipitation:
MYCN; Santa Cruz Cat #sc-53993 validated by shRNA
BRCA1; Bethyl Laboratories Cat #A300-000A validated by BRCA1; Santa Cruz Cat #sc-514797 and by siRNA and shRNA
RNAPII (RPB1); #sc-899; N-20 validated by RNAPII (RPB1); Santa Cruz Cat #sc-17798; A-10

Antibody for DRIP:
Anti DNA-RNA Hybrid; Boguslawski, S. J. et al. Characterization of monoclonal antibody to DNA.RNA and its application to immunodetection of hybrids. Journal of immunological methods 89, 123-130 and Anti DNA-RNA Hybrid; Kerafast Cat #ENH001 S9.6 validated by RNaseH treatment

Eukaryotic cell lines

Policy information about cell lines

Cell line source(s)

Human neuroblastoma: IMR-32 (M. Schwab)
Human neuroblastoma: IMR-5 (A. Eggert)
Human neuroblastoma: SMS-KAN (A. Eggert)
Human neuroblastoma: SH-EP (M. Schwab)
Pseudoviral Particle Producer cell line: HEK293TN (ATCC CRT-11268)
Retrovirus packaging cell line: Plat-E (B. von Eyss)
Mouse pancreatic cancer cell line: KPC (J. Siveke)
Mouse embryonic fibroblast: NIH3T3 (D. Murphy)

Authentication

Authentification of the cell lines used was done by STR profile testing, working according to the human cell line authentication standard published by ANSI.

Mycoplasma contamination

All cell lines were routinely tested for mycoplasma contamination.

Commonly misidentified lines
(See ICLAC register)

Non of the used cell lines is listed in the ICLAC register.

Method-specific reporting

n/a	Involved in the study
☐	☒ ChIP-seq
☐	☒ Flow cytometry
☒	☐ Magnetic resonance imaging

ChIP-seq

Data deposition

☒ Confirm that both raw and final processed data have been deposited in a public database such as GEO.

☒ Confirm that you have deposited or provided access to graph files (e.g. BED files) for the called peaks.

Data access links
May remain private before publication.

GEO: GSE111905
GEO: GSE113861

Files in database submission

ChIPseq_minusOHT_RNAPIIN20.bedgraph
ChIPseq_plusOHT_RNAPIIN20.bedgraph
ChIPseq_minusOHT_RNAPIIpSer2.bedgraph
ChIPseq_plusOHT_RNAPIIpSer2.bedgraph
ChIPseq_minusOHT_inputRNAPII.bedgraph
ChIPseq_plusOHT_inputRNAPII.bedgraph
ChIPseq_plusOHT_shBRCA1#1_input.bedgraph
ChIPseq_minusOHT_shBRCA1#1_RNAPIIN20.bedgraph
ChIPseq_plusOHT_shBRCA1#1_RNAPIIN20.bedgraph
ChIPseq_minusOHT_shSCR_RNAPIIN20.bedgraph

ChIPseq_plusOHT_shSCR_RNAPIIN20.bedgraph
ChIPseq_minusOHT_shBRCA1#1_RNAPIIpSer2.bedgraph
ChIPseq_plusOHT_shBRCA1#1_RNAPIIpSer2.bedgraph
ChIPseq_minusOHT_shSCR_RNAPIIpSer2.bedgraph
ChIPseq_plusOHT_shSCR_RNAPIIpSer2.bedgraph
ChIPseq_minusOHT_shBRCA1#2_RNAPIIA10.bedgraph
ChIPseq_plusOHT_shBRCA1#2_RNAPIIA10.bedgraph
ChIPseq_minusOHT_shSCR_RNAPIIA10.bedgraph
ChIPseq_plusOHT_shSCR_RNAPIIA10.bedgraph
ChIPseq_plusOHT_shBRCA1#2_input.bedgraph
ChIPseq_minusOHT_BRCA1.bedgraph
ChIPseq_plusOHT_BRCA1.bedgraph
ChIPseq_minusOHT_RPA1.bedgraph
ChIPseq_plusOHT_RPA1.bedgraph
ChIPseq_minusOHT_input.bedgraph
ChIPseq_plusOHT_input.bedgraph
ChIPseq_pWZL-NMYCwt_BRCA1.bedgraph
ChIPseq_pWZL-empty_BRCA1.bedgraph
ChIPseq_pWZL-NMYCwt_input.bedgraph
ChIPseq_minusOHT_NMYC.bedgraph
ChIPseq_plusOHT_NMYC.bedgraph
ChIPseq_minusOHT_inputNMYC.bedgraph
ChIPseq_plusOHT_inputNMYC.bedgraph
ChIPseq_2_minusOHT_BRCA1.bedgraph
ChIPseq_2_minusOHT_etoposide_BRCA1.bedgraph
ChIPseq_2_plusOHT_etoposide_BRCA1.bedgraph
ChIPseq_2_minusOHT_flavopiridol_BRCA1.bedgraph
ChIPseq_2_plusOHT_flavopiridol_BRCA1.bedgraph
ChIPseq_2_plusOHT_BRCA1.bedgraph
ChIPseq_2_input.bedgraph
ChIPseq_3_minusOHT_shBRCA1#1_DCP1A.bedgraph
ChIPseq_3_plusOHT_shBRCA1#1_DCP1A.bedgraph
ChIPseq_3_minusOHT_shSCR_DCP1A.bedgraph
ChIPseq_3_plusOHT_shSCR_DCP1A.bedgraph
ChIPseq_3_input.bedgraph
ChIPseq_pRRL-NMYC_input.bedgraph
ChIPseq_pRRL-NMYC_NMYC.bedgraph
ChIP-Rxseq_spikeNorm_input.bedgraph
ChIP-Rxseq_spikeNorm_input.bedgraph
ChIP-Rxseq_spikeNorm_input.bedgraph
ChIP-Rxseq_spikeNorm_input.bedgraph
ChIP-Rxseq_spikeNorm_minusOHT_shBRCA1#1_NMYC.bedgraph
ChIP-Rxseq_spikeNorm_plusOHT_shBRCA1#1_NMYC.bedgraph
ChIP-Rxseq_spikeNorm_minusOHT_shSCR_NMYC.bedgraph
ChIP-Rxseq_spikeNorm_plusOHT_shSCR_NMYC.bedgraph
ChIP-Rxseq_2_spikeNorm_input.bedgraph
ChIP-Rxseq_2_spikeNorm_input.bedgraph
ChIP-Rxseq_2_spikeNorm_input.bedgraph
ChIP-Rxseq_2_spikeNorm_input.bedgraph
ChIP-Rxseq_2_spikeNorm_minusOHT_shBRCA1#1_RNAPII.bedgraph
ChIP-Rxseq_2_spikeNorm_plusOHT_shBRCA1#1_RNAPII.bedgraph
ChIP-Rxseq_2_spikeNorm_minusOHT_shSCR_RNAPII.bedgraph
ChIP-Rxseq_2_spikeNorm_plusOHT_shSCR_RNAPII.bedgraph
RNAseq_SH-EP-NMYCER_shBRCA1_countmatrix.txt
RNAseq_2_SH-EP-NMYCER_shBRCA1_countmatrix.txt
GROseq_SH-EP-NMYCER.bw
shRNAseq_counttable_pool1_represented_only.csv
shRNAseq_counttable_pool2_represented_only.csv
ChIPseq_minusOHT_RNAPIIN20.bam
ChIPseq_plusOHT_RNAPIIN20.bam
ChIPseq_minusOHT_RNAPIIpSer2.bam
ChIPseq_plusOHT_RNAPIIpSer2.bam
ChIPseq_minusOHT_inputRNAPII.bam
ChIPseq_plusOHT_inputRNAPII.bam
ChIPseq_plusOHT_shBRCA1#1_input.bam
ChIPseq_minusOHT_shBRCA1#1_RNAPIIN20.bam
ChIPseq_plusOHT_shBRCA1#1_RNAPIIN20.bam
ChIPseq_minusOHT_shSCR_RNAPIIN20.bam
ChIPseq_plusOHT_shSCR_RNAPIIN20.bam
ChIPseq_minusOHT_shBRCA1#1_RNAPIIpSer2.bam
ChIPseq_plusOHT_shBRCA1#1_RNAPIIpSer2.bam
ChIPseq_minusOHT_shSCR_RNAPIIpSer2.bam
ChIPseq_plusOHT_shSCR_RNAPIIpSer2.bam
ChIPseq_minusOHT_shBRCA1#2_RNAPIIA10.bam
ChIPseq_plusOHT_shBRCA1#2_RNAPIIA10.bam

ChIPseq_minusOHT_shSCR_RNAPIIA10.bam
ChIPseq_plusOHT_shSCR_RNAPIIA10.bam
ChIPseq_plusOHT_shBRCA1#2_input.bam
ChIPseq_minusOHT_BRCA1.bam
ChIPseq_plusOHT_BRCA1.bam
ChIPseq_minusOHT_RPA1.bam
ChIPseq_plusOHT_RPA1.bam
ChIPseq_minusOHT_input.bam
ChIPseq_plusOHT_input.bam
ChIPseq_pWZL-NMYCwt_BRCA1.bam
ChIPseq_pWZL-empty_BRCA1.bam
ChIPseq_pWZL-NMYCwt_input.bam
ChIPseq_minusOHT_NMYC.bam
ChIPseq_plusOHT_NMYC.bam
ChIPseq_minusOHT_inputNMYC.bam
ChIPseq_plusOHT_inputNMYC.bam
RNAseq_minusOHT_shBRCA1#1_rep1.bam
RNAseq_minusOHT_shBRCA1#1_rep2.bam
RNAseq_minusOHT_shBRCA1#1_rep3.bam
RNAseq_plusOHT_shBRCA1#1_rep1.bam
RNAseq_plusOHT_shBRCA1#1_rep2.bam
RNAseq_plusOHT_shBRCA1#1_rep3.bam
RNAseq_minusOHT_shSCR_rep1.bam
RNAseq_minusOHT_shSCR_rep2.bam
RNAseq_plusOHT_shSCR_rep1.bam
RNAseq_plusOHT_shSCR_rep2.bam
RNAseq_plusOHT_shSCR_rep3.bam
RNAseq_minusOHT_shBRCA1#2_rep1.bam
RNAseq_minusOHT_shBRCA1#2_rep2.bam
RNAseq_minusOHT_shBRCA1#2_rep3.bam
RNAseq_plusOHT_shBRCA1#2_rep1.bam
RNAseq_plusOHT_shBRCA1#2_rep2.bam
RNAseq_plusOHT_shBRCA1#2_rep3.bam
RNAseq_2_minusOHT_shSCR_rep1.bam
RNAseq_2_plusOHT_shSCR_rep1.bam
RNAseq_2_minusOHT_shBRCA1#2_rep1.bam
RNAseq_2_plusOHT_shBRCA1#2_rep1.bam
RNAseq_2_minusOHT_shBRCA1#1_rep1.bam
RNAseq_2_plusOHT_shBRCA1#1_rep1.bam
RNAseq_2_minusOHT_shSCR_rep2.bam
RNAseq_2_plusOHT_shSCR_rep2.bam
RNAseq_2_minusOHT_shBRCA1#2_rep2.bam
RNAseq_2_plusOHT_shBRCA1#2_rep2.bam
RNAseq_2_minusOHT_shBRCA1#1_rep2.bam
RNAseq_2_plusOHT_shBRCA1#1_rep2.bam
RNAseq_2_minusOHT_shSCR_rep3.bam
RNAseq_2_plusOHT_shSCR_rep3.bam
RNAseq_2_minusOHT_shBRCA1#2_rep3.bam
RNAseq_2_plusOHT_shBRCA1#2_rep3.bam
RNAseq_2_minusOHT_shBRCA1#1_rep3.bam
RNAseq_2_plusOHT_shBRCA1#1_rep3.bam
GROseq_SH-EP-NMYCER.fastq
ChIPseq_2_minusOHT_BRCA1.bam
ChIPseq_2_minusOHT_etoposide_BRCA1.bam
ChIPseq_2_plusOHT_etoposide_BRCA1.bam
ChIPseq_2_minusOHT_flavopiridol_BRCA1.bam
ChIPseq_2_plusOHT_flavopiridol_BRCA1.bam
ChIPseq_2_plusOHT_BRCA1.bam
ChIPseq_2_input.bam
ChIPseq_3_minusOHT_shBRCA1#1_DCP1A.bam
ChIPseq_3_plusOHT_shBRCA1#1_DCP1A.bam
ChIPseq_3_minusOHT_shSCR_DCP1A.bam
ChIPseq_3_plusOHT_shSCR_DCP1A.bam
ChIPseq_3_input.bam
ChIPseq_pRRL-NMYC_input.bam
ChIPseq_pRRL-NMYC_NMYC.bam
ChIP-Rxseq_minusOHT_shBRCA1#1_input.fastq
ChIP-Rxseq_plusOHT_shBRCA1#1_input.fastq
ChIP-Rxseq_minusOHT_shSCR_input.fastq
ChIP-Rxseq_plusOHT_shSCR_input.fastq
ChIP-Rxseq_minusOHT_shBRCA1#1_NMYC.fastq
ChIP-Rxseq_plusOHT_shBRCA1#1_NMYC.fastq
ChIP-Rxseq_minusOHT_shSCR_NMYC.fastq
ChIP-Rxseq_plusOHT_shSCR_NMYC.fastq
ChIP-Rxseq_2_minusOHT_shBRCA1#1_input.fastq

ChIP-Rxseq_2_plusOHT_shBRCA1#1_input.fastq
ChIP-Rxseq_2_minusOHT_shSCR_input.fastq
ChIP-Rxseq_2_plusOHT_shSCR_input.fastq
ChIP-Rxseq_2_minusOHT_shBRCA1#1_RNAPII.fastq
ChIP-Rxseq_2_plusOHT_shBRCA1#1_RNAPII.fastq
ChIP-Rxseq_2_minusOHT_shSCR_RNAPII.fastq
ChIP-Rxseq_2_plusOHT_shSCR_RNAPII.fastq
shRNAseq_pool1_EU_rep1.bam
shRNAseq_pool1_EU_rep2.bam
shRNAseq_pool1_LU_rep1.bam
shRNAseq_pool1_LU_rep2.bam
shRNAseq_pool1_LS_rep1.bam
shRNAseq_pool1_LS_rep2.bam
shRNAseq_pool2_EU_rep1.bam
shRNAseq_pool2_EU_rep2.bam
shRNAseq_pool2_LU_rep1.bam
shRNAseq_pool2_LU_rep2.bam
shRNAseq_pool2_LS_rep1.bam
shRNAseq_pool2_LS_rep2.bam

Genome browser session
(e.g. UCSC)

Graphical files can be downloaded from GEO.

Methodology

Replicates

ChIP-seq experiment were done in biological duplicates (n=2) except ChIP-seq experiments for cells treated with etoposide and flavopiridol, cells expressing ectopic MYCN and MYCN recruitment in BRCA-depleted cells. For experiments involving shRNA-mediated depletion we used two independent shRNAs and binding of total RNAPII was meassured with two different antibodies. For all ChIP-seq experiments we validated effects in independent manual ChIPs.

Sequencing depth

sample sequenced mapped(hg19_or_hg19/mm10) read_length library
ChIPseq_pWZL-empty_BRCA1 12086545 10737602 75 single-end
ChIPseq_pWZL-NMYCwt_BRCA1 13036367 10625942 75 single-end
ChIPseq_pWZL-NMYCwt_input 7793535 6671908 75 single-end
ChIPseq_minusOHT_BRCA1 16587283 11469987 75 single-end
ChIPseq_plusOHT_BRCA1 16587283 9587893 75 single-end
ChIPseq_minusOHT_input 16587283 7835858 75 single-end
ChIPseq_plusOHT_input 16587283 11868755 75 single-end
ChIPseq_minusOHT_NMYC 33482360 29460120 75 single-end
ChIPseq_plusOHT_NMYC 39818452 35612423 75 single-end
ChIPseq_minusOHT_inputNMYC 41384321 38496948 75 single-end
ChIPseq_plusOHT_inputNMYC 37955890 35140600 75 single-end
ChIPseq_minusOHT_RNAPIIN20 16138999 15245575 75 single-end
ChIPseq_plusOHT_RNAPIIN20 18690867 17355906 75 single-end
ChIPseq_minusOHT_RNAPIIpSer2 16138999 16138999 75 single-end
ChIPseq_plusOHT_RNAPIIpSer2 18690867 17677576 75 single-end
ChIPseq_minusOHT_inputRNAPII 16138999 14531293 75 single-end
ChIPseq_plusOHT_inputRNAPII 18690867 17500841 75 single-end
ChIPseq_minusOHT_shBRCA1#1_RNAPIIN20 34296073 32200056 75 single-end
ChIPseq_plusOHT_shBRCA1#1_RNAPIIN20 21108901 19730324 75 single-end
ChIPseq_minusOHT_shSCR_RNAPIIN20 44186260 41101795 75 single-end
ChIPseq_plusOHT_shSCR_RNAPIIN20 44250392 40948560 75 single-end
ChIPseq_minusOHT_shBRCA1#1_RNAPIIpSer2 25887469 23720389 75 single-end
ChIPseq_plusOHT_shBRCA1#1_RNAPIIpSer2 27582822 25879716 75 single-end
ChIPseq_minusOHT_shSCR_RNAPIIpSer2 42706390 39226410 75 single-end
ChIPseq_plusOHT_shSCR_RNAPIIpSer2 23834912 22349830 75 single-end
ChIPseq_plusOHT_shBRCA1#1_input 28689782 24516701 75 single-end
ChIPseq_minusOHT_shBRCA1#2_RNAPIIA10 26013346 23293052 75 single-end
ChIPseq_plusOHT_shBRCA1#2_RNAPIIA10 28754102 20921667 75 single-end
ChIPseq_minusOHT_shSCR_RNAPIIA10 26364369 23769637 75 single-end
ChIPseq_plusOHT_shSCR_RNAPIIA10 30484530 27544608 75 single-end
ChIPseq_plusOHT_shBRCA1#2_input 58971564 53313062 75 single-end
ChIPseq_2_input 114559030 100319588 75 single-end
ChIPseq_2_minusOHT_BRCA1 18787288 13988876 75 single-end
ChIPseq_2_minusOHT_etoposide_BRCA1 49738797 38819992 75 single-end
ChIPseq_2_minusOHT_flavopiridol_BRCA1 23903913 17203530 75 single-end
ChIPseq_2_plusOHT_BRCA1 42044458 20857454 75 single-end
ChIPseq_2_plusOHT_etoposide_BRCA1 35557002 29124877 75 single-end
ChIPseq_2_plusOHT_flavopiridol_BRCA1 19486390 15925628 75 single-end
ChIPseq_3_input 30049768 27581387 75 single-end
ChIPseq_3_minusOHT_shBRCA1#1_DCP1A 18606861 16134850 75 single-end
ChIPseq_3_minusOHT_shSCR_DCP1A 15083377 13287649 75 single-end
ChIPseq_3_plusOHT_shBRCA1#1_DCP1A 24769209 20629831 75 single-end
ChIPseq_3_plusOHT_shSCR_DCP1A 19065800 16542937 75 single-end

ChIPseq_pRRL-NMYC_NMYC 12646344 8117373 75 single-end
ChIPseq_pRRL-NMYC_input 27917377 23428066 75 single-end
ChIP-Rxseq_minusOHT_shBRCA1#1_NMYC 31507087 22426624/7020561 75 single-end
ChIP-Rxseq_minusOHT_shBRCA1#1_input 11329347 7734694/2502592 75 single-end
ChIP-Rxseq_minusOHT_shSCR_NMYC 36309509 25840150/8307547 75 single-end
ChIP-Rxseq_minusOHT_shSCR_input 7231546 4940847/1975886 75 single-end
ChIP-Rxseq_plusOHT_shBRCA1#1_NMYC 35058145 27468628/5366969 75 single-end
ChIP-Rxseq_plusOHT_shBRCA1#1_input 7294141 5628194/1212174 75 single-end
ChIP-Rxseq_plusOHT_shSCR_NMYC 31721948 25344939/4427375 75 single-end
ChIP-Rxseq_plusOHT_shSCR_input 9087667 7110141/1414173 75 single-end
ChIP-Rxseq_2_minusOHT_shBRCA1#1_input 1968851 1522795/194448 75 single-end
ChIP-Rxseq_2_plusOHT_shBRCA1#1_input 1280465 1024218/124429 75 single-end
ChIP-Rxseq_2_minusOHT_shSCR_input 1531348 1195410/230550 75 single-end
ChIP-Rxseq_2_plusOHT_shSCR_input 1790886 1393478/276852 75 single-end
ChIP-Rxseq_2_minusOHT_shBRCA1#1_RNAPII 10206153/8267783 1271372 75 single-end
ChIP-Rxseq_2_plusOHT_shBRCA1#1_RNAPII 11414138 9147648/1310232 75 single-end
ChIP-Rxseq_2_minusOHT_shSCR_RNAPII 64910882 49552944/10971155 75 single-end
ChIP-Rxseq_2_plusOHT_shSCR_RNAPII 41670973 31948527/7048272 75 single-end

Antibodies

MYCN; Santa Cruz Cat #sc-53993
BRCA1; Bethyl Laboratories Cat #A300-000A
RNAPII (RPB1); Santa Cruz Cat #sc-899
RNAPII (RPB1); Santa Cruz Cat #sc-17798
p-RNAPII (Ser2); abcam Cat #ab5095
DCP1A; Santa Cruz #sc-100706

Peak calling parameters

Peak calling for BRCA1, MYCN and total RNAPII with MACS14 was performed with the corresponding input sample as control and with variable settings for duplicates ("--keep-dup"; ("antibody"/"biological condition"/"value"): BRCA1 +/-4-OHT 5; BRCA1 +/-4-OHT,+/-flavopiridol,+/-etoposide 3; MYCN +/-4-OHT 5; DCP1A +/-4-OHT,+/-shBRCA1 1; MYCN pRRL-MYCN: 1; BRCA1 pWZL-MYCN/pWZL-empty 5; total RNAPII EtOH 5) and p-value ("--pvalue"; ("antibody"/"biological condition"/"value"): BRCA1 +/-4-OHT 1e-6; BRCA1 +/-4-OHT,+/-flavopiridol,+/-etoposide 1e-7; MYCN +/-4-OHT 1e-11; DCP1A +/-4-OHT,+/-shBRCA1 1e-6; MYCN pRRL-MYCN 1e-9; BRCA1 pWZL-MYCN/pWZL-empty 1e-9; total-RNAPII EtOH 1e-14). Peak calling of the MYCN-ChIP-Rx samples was done with MACS14 (keep-dup: 1, p-value: 1e-10) with a separate peak calling for the corresponding input sample using same parameters as the "treat" sample. Overlapping peaks in the input were then subtracted from the MYCN-ChIP-Rx samples.

Data quality

Overall sequencing quality was controlled using the FastQC script.
Number of MACS14 called peaks (number in brackets indicates peaks at an FDR of 0.05):
BRCA1 4-OHT: 24,549 (22,469)
BRCA1 EtOH: 1,243 (1)
MYCN 4-OHT: 30,214 (30,214)
MYCN EtOH: 47,165 (47,107)
BRCA1 pWZL-MYCN: 27,595 (27,514)
BRCA1 pWZL-empty: 1,533 (0)
MYCN pRRL-MYCN: 18,800 (18,747)
MYCN EtOH_shSCR: 282 (na)
MYCN 4-OHT_shSCR: 1,480 (na)
MYCN EtOH_shBRCA1: 290 (na)
MYCN 4-OHT_shBRCA1: 446 (na)
input_EtOH_4-OHT_shSCR_shBRCA1: 373 (na)
RNAPII EtOH: 44,903 (44,903)
BRCA1_exp2 EtOH: 3,298 (2,387)
BRCA1_exp2 4-OHT: 29,033 (28,806)
BRCA1_exp2 EtOH_flavopiridol: 10,625 (10,397)
BRCA1_exp2 4-OHT_flavopiridol: 15,072 (14,997)
BRCA1_exp2 EtOH_etoposide: 9,085 (9,053)
BRCA1_exp2 4-OHT_etoposide: 9,609 (9,598)
DCP1A EtOH_shSCR: 11,472 (11,274)
DCP1A 4-OHT_shSCR: 2,505 (2,505)
DCP1A EtOH_shBRCA1: 8,768 (8,768)
DCP1A 4-OHT_shBRCA1: 487 (25)
ChIP-Rx: NMYC EtOH shSCR: 53 (na)
ChIP-Rx: NMYC OHT shSCR: 1223 (na)
ChIP-Rx: NMYC EtOH shBRCA1: 54 (na)
ChIP-Rx: NMYC OHT shBRCA1: 196 (na)

Software

FASTQ Generation software v1.0.0 http://illumina.com
FastQC v0.11.3 http://www.bioinformatics.babraham.ac.uk/projects/fastqc/
Bowtie v1.2 Langmead B, Trapnell C, Pop M, Salzberg SL. Ultrafast and memory-efficient alignment of short DNA sequences to the human genome. Genome Biol 10:R25.
MACS v1.4.1 Zhang et al. Model-based Analysis of ChIP-Seq (MACS). Genome Biol (2008) vol. 9 (9) pp. R137
BEDtools v2.26.0 Quinlan AR, Hall IM. BEDTools: a flexible suite of utilities for comparing genomic features. Bioinformatics. 2010;26(6):841-842.
SAMtools v1.3 Li H., Handsaker B., Wysoker A., Fennell T., Ruan J., Homer N., Marth G., Abecasis G., Durbin R. and 1000 Genome Project Data Processing Subgroup (2009) The Sequence alignment/map (SAM) format and SAMtools.

Bioinformatics, 25, 2078-9. [PMID: 19505943]
DeepTools v2.3.5 Ramírez F, Dündar F, Diehl S, Grüning BA, Manke T. deepTools: a flexible platform for exploring deep-sequencing data. Nucleic Acids Res. 2014 Jul;42:W187-91.
NGSplot v2.61 Shen, L., Shao, N., Liu, X. and Nestler, E. (2014) ngs.plot: Quick mining and visualization of next-generation sequencing data by integrating genomic databases, BMC Genomics, 15, 284.
Integrated Genome Browser v9.0.0 Freese NH, Norris DC, Loraine AE. Integrated genome browser: visual analytics platform for genomics. Bioinformatics. Epub: 2016, March 16; 1-7. 10.1093/bioinformatics/btw069
MEME Suite v4.10.1 Timothy L. Bailey, Mikael Bodén, Fabian A. Buske, Martin Frith, Charles E. Grant, Luca Clementi, Jingyuan Ren, Wilfred W. Li, William S. Noble, "MEME SUITE: tools for motif discovery and searching", Nucleic Acids Research, 37:W202-W208, 2009.
skewR Ginno, P. A., Lott, P. L., Christensen, H. C., Korf, I. & Chedin, F. R-loop formation is a distinctive characteristic of unmethylated human CpG island promoters. Mol Cell 45, 814-825, doi:10.1016/j.molcel.2012.01.017 (2012).
CASAVA v1.7 http://emea.support.illumina.com/downloads/casava_software_version_18_user_guide_(15011196_b).html?langsel=/de/
ImageJ v1.50j http://imagej.nih.gov/ij

Flow Cytometry

Plots

Confirm that:

☒ The axis labels state the marker and fluorochrome used (e.g. CD4-FITC).

☒ The axis scales are clearly visible. Include numbers along axes only for bottom left plot of group (a 'group' is an analysis of identical markers).

☒ All plots are contour plots with outliers or pseudocolor plots.

☒ A numerical value for number of cells or percentage (with statistics) is provided.

Methodology

Sample preparation	Bromodeoxyuridine (BrdU) -Propidiumiodide (-PI) -FACS was performed as described previously (Schulein-Volk et al., 2014). Subconfluent cells were labelled with 20 µM 5-Bromo-2'-deoxyuridine (BrdU, Sigma-Aldrich) for 1 h. Cells were harvested, washed with ice-cold PBS and fixed in 80 % ethanol overnight at -20°C. Cells were washed with cold PBS and incubated in 2 M HCl/0.5 % Triton X-100 for 30 min at room temperature. Cell pellets were neutralized by incubating with Na2B4O7. The pellet was incubated with Anti-BrdU-FITC antibody (Becton-Dickinson) diluted in 100 µl 1 % BSA, 0.5 % Tween-20 in PBS for 30 minutes at room temperature in the dark. After washing with PBS, the cells were re-suspended in PBS with RNAse A (24 µg ml-1) and propidium iodide (PI, 54 µM) and incubated for 30 min at 37°C. For PI-FACS cells were harvested by trypsinization, washed with cold PBS and fixed in 80 % ethanol overnight at –20 °C. After washing with PBS, the cells were re-suspended in PBS with RNaseA (24 µg ml-1) and PI (54 µM) and incubated for 30 min at 37°C. For AnnexinV-PI-FACS cells were harvested together with the supernatant by trypsinzation and washed with cold PBS. Cell pellet was re-suspended in 100 µl 1x AnnexinV-binding buffer (10 mM HEPES pH 7.4, 140 mM NaCl, 2.5 mM CaCl2) and 2 µl AnnexinV/Pacific Blue dye and incubated for 15 min at room temperature in the dark. Afterwards 400 µl 1x binding buffer and 5 µl PI (54 µM) was added and the samples were stored cold and dark until analysis.
Instrument	BD FACSCanto II flow cytometer
Software	BD FACSDIVA Software v6.1.2
Cell population abundance	For each experiment a total of 20,000 cells was analyzed.
Gating strategy	Gates and regions are placed around populations of cells with special characteristics.

☐ Tick this box to confirm that a figure exemplifying the gating strategy is provided in the Supplementary Information.